

# Integrated Communications and Localization for Massive MIMO LEO Satellite Systems

Li You, Xiaoyu Qiang, Yongxiang Zhu, Fan Jiang, Christos G. Tsinos, Wenjin Wang, Henk Wymeersch, Xiqi Gao, and Björn Ottersten

**Abstract**—Integrated communications and localization (ICAL) will play an important part in future sixth generation (6G) networks for the realization of Internet of Everything (IoE) to support both global communications and seamless localization. Massive multiple-input multiple-output (MIMO) low earth orbit (LEO) satellite systems have great potential in providing wide coverage with enhanced gains, and thus are strong candidates for realizing ubiquitous ICAL. In this paper, we develop a wideband massive MIMO LEO satellite system to simultaneously support wireless communications and localization operations in the down-link. In particular, we first characterize the signal propagation properties and derive a localization performance bound. Based on these analyses, we focus on the hybrid analog/digital precoding design to achieve high communication capability and localization precision. Numerical results demonstrate that the proposed ICAL scheme supports both the wireless communication and localization operations for typical system setups.

**Index Terms**—Integrated communications and localization, 6G, non-geostationary satellite, LEO satellite, massive MIMO, hybrid precoding, squared position error bound.

## I. INTRODUCTION

Fifth generation (5G) wireless networks are under deployment and the basic functionalities and capabilities are defined within the 5G standard [2]. However, there still exist many requirements that 5G networks may not satisfy, and sixth generation (6G) wireless networks are envisioned to offer seamless and ubiquitous coverage, higher communication capability and sensing/localization precision, and enhanced intelligence and security level, etc. [2]–[6]. One of the potential application scenarios of 6G networks is the integrated communications and localization (ICAL) on Internet of Everything (IoE),

including tracking of persons or robots in an industrial site, autonomous driving, emergency response, etc. In such use cases, communications and localization are simultaneously performed by jointly designing the signal waveform for shared spectrum on one hardware platform, to improve the utilization of resources [2], [5].

One of the common application cases for ICAL on IoE is the terrestrial network [7]–[9]. However, the ICAL functionality in a terrestrial network is unavailable in some areas where ground infrastructure is infeasible to deploy, or the signals are easily blocked [10]. In these scenarios, satellite networks can provide an attractive and cost effective complement for the terrestrial networks since they can provide larger coverage, and support wideband communications and more flexible localization for the areas that terrestrial networks might have coverage issues. Thus, satellite networks are expected to support global communications and seamless localization, and will play an essential role in performing ICAL for 6G networks [5], [11]–[13]. Generally, the satellite networks are divided into two categories, namely geostationary earth orbit (GEO) and non-GEO (NGEO) satellite networks [14]. The typical satellite networks, including several global navigation satellite systems (GNSSs), e.g., global positioning system (GPS), GLONASS, and BEIDOU, are commonly capable of offering primary navigation with wide converge [10]. Those satellite networks are generally based on GEO and medium earth orbit (MEO) satellites, and recently, low earth orbit (LEO) satellite constellations have attracted much attention in terms of their application into position, navigation, and timing (PNT) [15]. The LEO satellites are usually deployed at altitudes of 200 – 2000 km [16], and can be launched with low cost and high flexibility [10]. Moreover, due to lower propagation delay and smaller path loss and footprint, the LEO satellite networks can provide better communication capability and localization precision compared with GEO counterparts [10], [17]. So far, several large LEO satellite systems, e.g., OneWeb, SpaceX, have been launched by governments and corporations, and see a steady reduction in launch costs, which makes it possible to develop global LEO satellite systems, and complement GNSSs.

Massive multiple-input multiple-output (MIMO) can provide numerous degrees of freedom in both temporal and spatial domains [5]. Besides, it can provide sufficient link budget to potentially support wideband communications to mobile terminals without dedicated antennas, and provide multiple links to do localization and tracking. Therefore, it has gained much attention for pure communications and localization, to improve the spectral efficiency (SE) and the precision of localization

Copyright (c) 2015 IEEE. Personal use of this material is permitted. However, permission to use this material for any other purposes must be obtained from the IEEE by sending a request to pubs-permissions@ieee.org.

Part of this work was presented in ICC'2023 [1].

Li You, Xiaoyu Qiang, Yongxiang Zhu, Wenjin Wang, and Xiqi Gao are with the National Mobile Communications Research Laboratory, Southeast University, Nanjing 210096, China, and also with the Purple Mountain Laboratories, Nanjing 211100, China (e-mail: lyou@seu.edu.cn; xyqiang@seu.edu.cn; zhuyx@seu.edu.cn; wangwj@seu.edu.cn; xqgao@seu.edu.cn).

Fan Jiang is with the Pengcheng Laboratory, Shenzhen 518000, China. He was with the School of Information Technology, Halmstad University, Halmstad 30118, Sweden (Email: jiangf02@pcl.ac.cn)

Christos G. Tsinos is with the National and Kapodistrian University of Athens, Evia, 34400, Greece and also with the Interdisciplinary Centre for Security, Reliability and Trust (SnT), University of Luxembourg, Luxembourg City 2721, Luxembourg (e-mail: ctsinos@uoa.gr).

Henk Wymeersch is with the Department of Electrical Engineering, Chalmers University of Technology, Gothenburg 41296, Sweden (e-mail: henkw@chalmers.se).

Björn Ottersten is with the Interdisciplinary Centre for Security, Reliability and Trust (SnT), University of Luxembourg, Luxembourg City 2721, Luxembourg (bjorn.ottersten@uni.lu).

[17]–[19], which motivates us to adopt the massive MIMO technology for ubiquitous ICAL [5], [8], [20]. However, the implementation of fully digital transceivers in massive MIMO requires a large number of radio frequency (RF) chains, and might lead to high power consumption. Generally, this issue can be circumvented by developing a hybrid precoding architecture [21]. Recently, AST SpaceMobile has reported the successful deployment of the 693-square-foot MIMO array on its BlueWalker 3 LEO satellite [22]. Motivated by this, we combine the LEO satellite networks with the employment of massive MIMO in 6G, to support ICAL with the terrestrial user terminals (UTs) in the remote areas [4].

In this work, we propose to implement ICAL in the massive MIMO LEO satellite systems, to trade-off between the communication capability and the localization precision, which are evaluated by the SE and the squared position error bound (SPEB), respectively [5]. Though the precoding designs for the downlink of the ICAL systems have been already investigated in the terrestrial networks [7]–[9], the signal propagation properties in such systems differs from that of the LEO satellite ones, and thus can not be applied directly. Specifically, owing to the mobility of the transceivers and the long satellite-to-UTs distance, there exist large Doppler shifts and a long propagation latency in the considered scenario [17], [23]. Thus, the instantaneous channel state information (iCSI) between the satellite and the UTs is time-varying, which may be difficult to estimate. Moreover, the estimated iCSI might be outdated [24], which makes it challenging to use iCSI for downlink precoding in such system. Motivated by these characteristics, we investigate the precoding design by exploiting the statistical CSI (sCSI), which is relatively slow-varying.

Inspired by the aforementioned motivations, a hybrid analog/digital transmitter is proposed for wideband massive MIMO LEO satellite systems to perform ubiquitous ICAL by exploiting sCSI. The main contributions of the paper are summarized as follows:

- We investigate the upper bound of the ergodic SE expression. Besides, we derive a closed-form Cramér-Rao lower bound (CRLB) for the channel parameters of the considered systems, based on which the SPEB is derived to measure the performance of the downlink localization.
- We investigate the hybrid precoders multi-objective optimization for the considered systems, to trade-off between the communication capability and the localization precision, based on the SE and the SPEB metrics, respectively.
- We develop a hybrid precoding strategy and jointly design the signal waveform based on sCSI, to simultaneously perform communications and localization, and guarantee good performance in terms of both the SE as well as the SPEB metrics, respectively.

#### A. Related Works

*Communications* – So far, the communications for the LEO satellite scenarios have been intensively investigated. In [17], the authors have formulated a massive MIMO communication scheme for both uplink and downlink of the LEO satellite systems based on the average signal-to-leakage-plus-noise ratio

(ASLNR) and average signal-to-interference-plus-noise ratio (ASINR) maximization criteria, respectively. The downlink precoding designs for both fully digital and hybrid transmitters have been studied in [12], [24], [25], to maximize the downlink SE or the energy efficiency performance. Besides, joint user scheduling and beamforming frameworks have been investigated for the downlink of the massive MIMO LEO satellite systems [26], [27]. In [28], the authors focused on the research of the uplink transmit design for the massive MIMO LEO satellite systems.

*Localization* – Wireless localization can be performed with single anchor or multiple anchors, both of which have been extensively investigated in the terrestrial systems. In [29], [30], the authors have presented theoretical analyses for multiple anchor localizations. The CRLB for single anchor localization has been derived for both two-dimensional (2D) and three-dimensional (3D) scenarios in [18], [31]. In [32], the authors have investigated the localization and orientation performance limits for the single anchor scenarios with massive MIMO transmission. In [33], the authors have studied the influence of synchronization errors and Doppler effects on single anchor localization systems.

*ICAL* – The existing ICAL studies mainly focus on terrestrial scenarios. In [7], [8], the authors have designed the beamforming vectors to simultaneously perform communications and localization during data transmission, based on rate maximization, SPEB minimization, or the transmission power minimization criteria. Besides, localization can not only be performed together with the data transmission, but also with the pilot transmission, at the same time of channel estimation. In [9], the authors have proposed a two-stage beamforming scheme, where in the first stage, pilot overhead signaling is minimized subject to localization precision constraints, and in the second stage, the data rate is maximized with the estimated CSI obtained from stage one.

#### B. Organization

The paper is organized as follows. Section II formulates the system model for the wideband massive MIMO LEO satellite ICAL system. The performance metrics for both communications and localization, i.e., SE and SPEB, are analyzed in Section III. An algorithmic framework is developed in Section IV to design the hybrid analog/digital precoders for the ICAL system enabling the trade-off between the communication and localization performance. Section V presents the simulation results and the paper is concluded briefly in Section VI.

#### C. Notations

Matrices and vectors are denoted by upper and lower case boldface letters, respectively.  $\mathbb{C}^{m \times n}$  represents the  $m \times n$ -dimension unitary space. The left-hand side of  $\triangleq$  is defined by the right-hand side.  $\otimes$  denotes the Kronecker product.  $\exp\{\cdot\}$  and  $\log\{\cdot\}$  are the exponential and logarithmic operators, respectively.  $\mathbf{I}_N$  stands for  $N \times N$  identity matrix.  $(\cdot)^T$ ,  $(\cdot)^*$ , and  $(\cdot)^H$  represent the transpose, conjugate, and conjugate transpose operations, respectively.  $|x|$ ,  $\angle x$ ,  $\Re\{x\}$ , and  $\lceil x \rceil$  denote the amplitude, the angle, the real part, and the ceiling

value of  $x$ , respectively. The circular symmetric complex-valued zero-mean Gaussian distribution with variance  $\sigma^2$  is given by  $\mathcal{CN}(0, \sigma^2)$ .  $\mathbb{E}\{\cdot\}$ ,  $\text{Tr}\{\cdot\}$ , and  $\text{blkdiag}\{\cdot\}$  represent the expectation, the trace, and the block diagonal operators.  $\text{rank}\{\mathbf{X}\}$  stands for the rank of the matrix  $\mathbf{X}$ .  $\|\cdot\|_2$  and  $\|\cdot\|_F$  denote the  $\ell_2$ -norm and Frobenius-norm, respectively. The  $(i, j)$ th element of the matrix  $\mathbf{A}$  is given by  $[\mathbf{A}]_{i,j}$ .  $\mathbf{A} \succeq \mathbf{B}$  refers to the positive semidefinite property of the matrix  $\mathbf{A} - \mathbf{B}$ .  $\partial$  denotes the partial derivative operation.

## II. SYSTEM MODEL

We propose to simultaneously perform communications and localization for the massive MIMO LEO satellite systems, as depicted in Fig. 1. The system is operated at carrier frequency

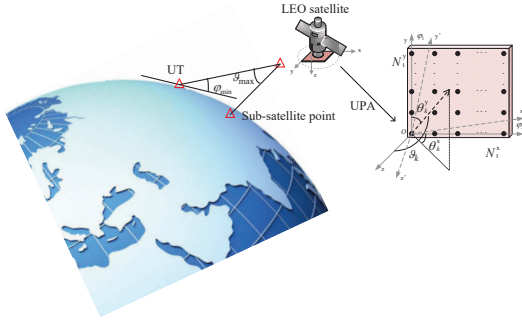


Fig. 1. 3D geometric model of the massive MIMO LEO satellite ICAL system with known satellite position and orientation, unknown UTs position.

$f_c$  and the corresponding wavelength is given by  $\lambda_c = c/f_c$ , where  $c$  denotes the speed of the light. We assume  $K$  single-antenna UTs, at unknown position  $\mathbf{p}_k = [p_k^x, p_k^y, p_k^z]^T$  and velocity  $\dot{\mathbf{p}}_k = [\dot{p}_k^x, \dot{p}_k^y, \dot{p}_k^z]^T$ ,  $k = 1, \dots, K$ , are served by a single LEO satellite with known position  $\mathbf{q} = [q^x, q^y, q^z]^T$  and orientation angle  $\mathbf{o} = [\varphi_1, \varphi_2]^T$ ,<sup>1</sup> where  $\varphi_2$  and  $\varphi_1$  refer to the rotation around positive  $y$ - and negative  $x'$ -axes,<sup>2</sup> respectively, as depicted in Fig. 1. We assume fixed positions and velocities of the UTs over the observed interval and update them according to the large movements of the UTs. A uniform planar array (UPA) of  $N_t = N_t^x N_t^y$  antennas with half-wavelength separation is applied at the LEO satellite transmitter, where  $N_t^x$  and  $N_t^y$  denote the number of antennas at the  $x$ - and  $y$ -axes, respectively. The satellite transmitter is supported by a hybrid precoder with  $N_{\text{rf}}$  ( $K \leq N_{\text{rf}} \leq N_t$ ) RF chains.

The orthogonal frequency division multiplex (OFDM) modulation is employed for the downlink wideband transmission of the LEO satellite ICAL systems to mitigate the inter-symbol interference [17], [18]. We denote  $B_w$  and  $T_s = 1/(2B_w)$  as the system bandwidth and the sampling period, respectively. In particular, we assume each frame consists of  $M_s$  slots, and there are  $M_{\text{sp}}$  and  $M_{\text{sd}}$  OFDM symbols used for pilot

<sup>1</sup>The orientation angle can be obtained and pre-compensated by, e.g., programmed tracking, accordingly with predicted movement of the LEO satellite [34].

<sup>2</sup>After a rotation by  $\varphi_2$  around positive  $y$ -axis, the  $y$ -coordinate does not change, i.e.,  $y' = y$ , while the  $x$ - and  $z$ -coordinates vary as  $x' = z \sin \varphi_2 + x \cos \varphi_2$  and  $z' = z \cos \varphi_2 - x \sin \varphi_2$ , respectively.

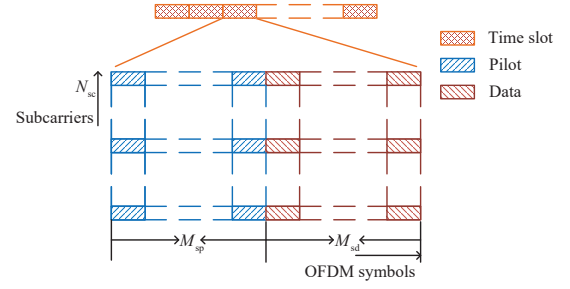


Fig. 2. The time-frequency structure for the transmitted pilot and data signals.

and data transmission in each slot, as depicted in Fig. 2. Thus, in each frame,  $M_p = M_{\text{sp}} M_s$  and  $M_d = M_{\text{sd}} M_s$  OFDM symbols are transmitted through the pilot and data transmission, respectively. Then, we assume  $N_{\text{sc}}$  subcarriers are employed over the system bandwidth  $B_w$ , and the length of the cyclic prefix (CP) is set as  $N_{\text{cp}}$ . Thus, we denote  $f_s$  as the subcarrier separation and the frequency of the  $n$ th subcarrier is given by  $f_n = (n - \frac{N_{\text{sc}}+1}{2})f_s$ ,  $n = 1, \dots, N_{\text{sc}}$ . Subsequently, the OFDM symbol length with and without CP is given by  $T = N_{\text{sc}}T_s + N_{\text{cp}}T_s$  and  $T_{\text{sc}} = N_{\text{sc}}T_s$ , respectively. In the following, let the subscript and superscript  $g \in \{\text{p}, \text{d}\}$  represent the pilot and data transmission, respectively.

An ICAL transmission protocol is developed for the LEO satellite systems. First, rough position knowledge of both the satellite and the UTs can be obtained at the LEO satellite side by, e.g., initial access or tracking [35], by exploiting which the satellite transmits precoded pilot and data signals to each UT. Then, the required channel parameters can be evaluated from the received pilot signals at the UT, and more precise localization knowledge can be derived from the estimated channel information [7], [18], [31], to further improve the localization precision and communication capacity.

### A. Channel Model

In the wideband massive MIMO LEO satellite ICAL systems, the UPA response is not only dependent on the angles-of-departure (AoD) information, but also the frequency. Then, the UPA response  $\mathbf{v}_{k,l}(f)$  for the  $l$ th propagation path of the  $k$ th UT at frequency  $f$  is given by [36]

$$\begin{aligned} \mathbf{v}_{k,l}(f) &= \mathbf{v}_{k,l}^x(f) \otimes \mathbf{v}_{k,l}^y(f) \\ &= \mathbf{v}_x(f, \boldsymbol{\theta}_{k,l}) \otimes \mathbf{v}_y(f, \boldsymbol{\theta}_{k,l}) \in \mathbb{C}^{N_t \times 1}, \end{aligned} \quad (1)$$

where  $\boldsymbol{\theta}_{k,l} = (\theta_{k,l}^x, \theta_{k,l}^y)$  denotes the AoD pair, as observed from Fig. 1. Besides, the array response vectors  $\mathbf{v}_x(f, \boldsymbol{\theta}_{k,l}) \in \mathbb{C}^{N_t^x \times 1}$  and  $\mathbf{v}_y(f, \boldsymbol{\theta}_{k,l}) \in \mathbb{C}^{N_t^y \times 1}$  of the  $x$ - and  $y$ -axes can be expressed as [17], [36]

$$\begin{aligned} \mathbf{v}_{k,l}^x(f) \triangleq \mathbf{v}_x(f, \boldsymbol{\theta}_{k,l}) &= \frac{1}{\sqrt{N_t^x}} \left[ 1 \exp\{-j\varpi \sin \theta_{k,l}^y \cos \theta_{k,l}^x\} \right. \\ &\quad \left. \cdots \exp\{-j\varpi(N_t^x - 1) \sin \theta_{k,l}^y \cos \theta_{k,l}^x\} \right]^T, \end{aligned} \quad (2)$$

$$\mathbf{v}_{k,l}^y(f) \triangleq \mathbf{v}_y(f, \boldsymbol{\theta}_{k,l}) = \frac{1}{\sqrt{N_t^y}} \left[ 1 \exp\{-j\varpi \cos \theta_{k,l}^y\} \cdots \right.$$

$$\exp\{-j\varpi(N_t^y - 1) \cos \theta_{k,l}^y\}^T, \quad (3)$$

where  $\varpi = \pi(1 + f/f_c)$ .

Generally, the LEO satellite is deployed at an altitude much higher than that of the scatterers around the UTs, then the AoD of each path for the channel associated with the  $k$ th UT is almost identical,<sup>3</sup> i.e.,  $\boldsymbol{\theta}_{k,l} \triangleq \boldsymbol{\theta}_k$ ,  $\forall l$ , and thus we have  $\mathbf{v}_{k,l}(f) = \mathbf{v}_k(f)$ ,  $\mathbf{v}_{k,l}^d(f) = \mathbf{v}_k^d(f) \in \mathbb{C}^{N_t^d \times 1}$ ,  $\forall l$ ,  $d \in \{x, y\}$ . Let  $\mathbf{v}_{k,n} \triangleq \mathbf{v}_k(f_n)$ ,  $\mathbf{v}_{k,n}^d \triangleq \mathbf{v}_k^d(f_n)$ , and then, with perfect time and frequency synchronization between the satellite and the UTs,<sup>4</sup> the effective channel vector  $\mathbf{h}_{k,m_g,n} \in \mathbb{C}^{N_t \times 1}$  for the  $k$ th UT over the  $n$ th subcarrier of the  $m_g$ th OFDM symbol is given by  $\mathbf{h}_{k,m_g,n} = \mathbf{h}_{k,m_g,n}^{\text{los}} + \mathbf{h}_{k,m_g,n}^{\text{nlos}}$  [24], where  $\mathbf{h}_{k,m_g,n}^{\text{los}}$  and  $\mathbf{h}_{k,m_g,n}^{\text{nlos}}$  denote the line-of-sight (LoS) and non-line-of-sight (NLoS) part of the channel, respectively, and they can be detailed as

$$\mathbf{h}_{k,m,n}^{\text{los}} = g_{k,m_g,n}^{\text{los}} \mathbf{v}_{k,n}, \quad (4)$$

$$\mathbf{h}_{k,m,n}^{\text{nlos}} = g_{k,m_g,n}^{\text{nlos}} \mathbf{v}_{k,n}. \quad (5)$$

Define  $g_{k,m_g,n} = g_{k,m_g,n}^{\text{los}} + g_{k,m_g,n}^{\text{nlos}}$ , where  $g_{k,m_g,n}^{\text{los}}$  and  $g_{k,m_g,n}^{\text{nlos}}$  denote the channel gains of the LoS and NLoS parts, respectively. Then, since there are numerous propagation paths,  $g_{k,m_g,n}$  can be approximated as the composition of a large number of independent and identically distributed components that follow the Rician distribution with Rician factor  $\kappa_k$  and average power  $\gamma_k = \mathbb{E}\{|g_{k,m_g,n}|^2\}$  [39]. In (4), the complex gain  $g_{k,m_g,n}^{\text{los}}$  is given by  $g_{k,m_g,n}^{\text{los}} = \alpha_k \exp\{j2\pi(\nu_k m_g T - n f_s \tau_k)\}$ ,<sup>5</sup> where  $\nu_k$  and  $\tau_k$  are Doppler shifts and propagation delay of the LoS path with the  $k$ th UT, respectively.<sup>6</sup> Besides,  $\alpha_k = \sqrt{\frac{\kappa_k \gamma_k}{1 + \kappa_k}} \exp\{j\phi_k\}$ , where  $\phi_k \in (0, 2\pi]$  is a random phase. In addition, in (5), the complex gain  $g_{k,m_g,n}^{\text{nlos}}$  follows that  $g_{k,m,n}^{\text{nlos}} \sim \mathcal{CN}(0, \frac{\gamma_k}{1 + \kappa_k})$ .

### B. Signal Model

We denote the transmitted pilot signal over the  $m_p$ th OFDM symbol as  $\{\mathbf{s}_{m_p,n}^{\text{p}}\}_{n=1}^{N_{\text{sc}}^{\text{p}}}$ , where  $\mathbf{s}_{m_p,n}^{\text{p}} = \{s_{m_p,n,1}^{\text{p}}, \dots, s_{m_p,n,K}^{\text{p}}\}$ ,  $m_p = 1, \dots, M_p$  and satisfies  $\mathbb{E}\{\mathbf{s}_{m_p,n}^{\text{p}}(\mathbf{s}_{m_p,n}^{\text{p}})^H\} = \mathbf{I}_K$ . Besides, the transmitted data signal over the  $m_d$ th OFDM symbol is denoted as  $\{\mathbf{s}_{m_d,n}^{\text{d}}\}_{n=1}^{N_{\text{sc}}^{\text{d}}}$ , where  $\mathbf{s}_{m_d,n}^{\text{d}} = \{s_{m_d,n,1}^{\text{d}}, \dots, s_{m_d,n,K}^{\text{d}}\}$ ,  $m_d = 1, \dots, M_d$ ,  $\mathbb{E}\{s_{m_d,n,k}^{\text{d}}\} = 0$

<sup>3</sup>For an orbit height of about 200 km, the AOD difference of the x- and y-axes are about  $0.03^\circ$  and  $0.01^\circ$  when the scatterers are spread at a maximum radius of 100 m, which can be negligible.

<sup>4</sup>The clock bias/synchronization errors of the different UTs are not considered in the models and algorithms of this work. In particular, synchronization can be assumed to be done by, e.g., a tracking algorithm or a joint localization and synchronization approach [37] for simplicity (Also, the downlink transmission is a second phase of a real-time transport protocol, so that the distance can be determined by the time-of-arrival). Besides, in this work, we assume perfect carrier frequency offset synchronization between the UTs and the satellite, which can be obtained and then compensated by e.g., a under-sampling approach [38].

<sup>5</sup>Note that this model is valid for moderate Doppler spreads for which inter-carrier-interference can be mitigated [40].

<sup>6</sup>The Doppler shift related to the mobility of the LEO satellite can be pre-compensated due to its deterministic time variation [41].

and  $\mathbb{E}\{s_{m_d,n,k}^{\text{d}}(s_{m'_d,n',k'}^{\text{d}})^*\} = \delta(m_d - m'_d)\delta(n - n')\delta(k - k')$  [7].

At the  $n$ th subcarrier over the  $m_g$ th OFDM symbol, the transmitted signal  $\mathbf{s}_{m_g,n}^g$  is first processed by a baseband precoder  $\mathbf{W}_{\text{BB},n} \in \mathbb{C}^{N_{\text{rf}} \times K}$  and then by an analog precoder  $\mathbf{W}_{\text{RF}} \in \mathbb{C}^{N_t \times N_{\text{rf}}}$  [42], as depicted in Fig. 3. Thus, the final transmission signal is given by  $\mathbf{x}_{m_g,n}^g = \mathbf{W}_{\text{RF}} \mathbf{W}_{\text{BB},n} \mathbf{s}_{m_g,n}^g = \mathbf{W}_n \mathbf{s}_{m_g,n}^g$ , where  $\mathbf{W}_n = [\mathbf{w}_{n,1}, \mathbf{w}_{n,2}, \dots, \mathbf{w}_{n,K}]$  is the equivalent hybrid precoding matrix. Then, the received pilot/data signal over the  $n$ th subcarrier of the  $m_g$ th OFDM symbol at the  $k$ th UT is given by

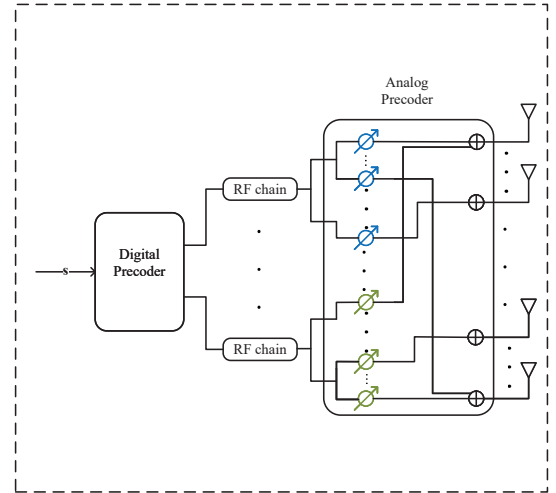
$$\mathbf{y}_{k,m_g,n}^g = \mathbf{h}_{k,m_g,n}^T \mathbf{W}_n \mathbf{s}_{m_g,n}^g + z_{k,m_g,n}^g, \quad (6)$$

where  $z_{k,m_g,n}^g \sim \mathcal{CN}(0, N_0)$ ,  $\forall k, m_g, n$ ,  $\forall g \in \{\text{p}, \text{d}\}$ .

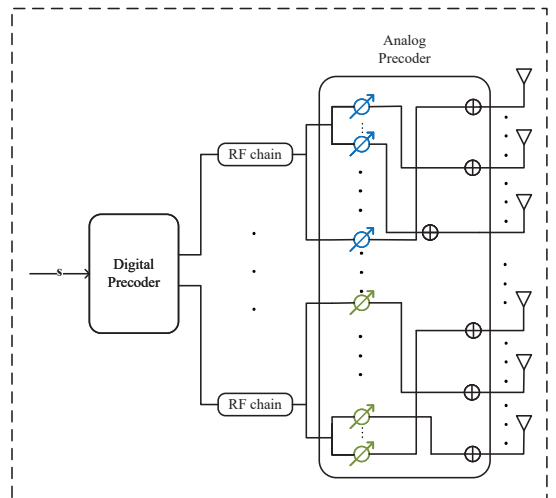
## III. PERFORMANCE METRICS

### A. Communication Spectral Efficiency

In the following, we first omit the OFDM symbol and subcarrier indices  $m_d$  and  $n$  for a clearer description of the



(a) Fully connected.



(b) Partially connected.

Fig. 3. Hybrid precoding architectures of the massive MIMO LEO satellite ICAL system.

channel statistical properties. During data transmission, the ergodic data rate for the  $k$ th UT is given by

$$R_k = \mathbb{E} \left\{ \log \left( 1 + \frac{|\mathbf{h}_k^T \mathbf{w}_k|^2}{\sum_{\ell \neq k} |\mathbf{h}_k^T \mathbf{w}_\ell|^2 + N_0} \right) \right\}. \quad (7)$$

Note that Monte Carlo method can be used to estimate the ergodic data rate. However, the computational complexity of the Monte Carlo method is extremely high, and the accurate iCSI is difficult to be obtained at the LEO satellite transmitter, as mentioned in the introduction, which motivates us to adopt sCSI. Based on the [43, Lemma 2], it can be concluded that the logarithmic expression inside the expectation operator of  $R_k$  is concave with respect to the matrix  $\mathbf{h}_k^* \mathbf{h}_k^T$  and thus, is upper bounded by

$$R_k \leq \bar{R}_k = \log \left( 1 + \frac{\mathbf{w}_k^H \mathbb{E} \{ \mathbf{h}_k^* \mathbf{h}_k^T \} \mathbf{w}_k}{\sum_{\ell \neq k} \mathbf{w}_\ell^H \mathbb{E} \{ \mathbf{h}_k^* \mathbf{h}_k^T \} \mathbf{w}_\ell} \right). \quad (8)$$

In (8), the expectation expression  $\mathbb{E} \{ \mathbf{h}_k^* \mathbf{h}_k^T \}$  represents the channel correlation matrix at the satellite side for the  $k$ th UT. Thus, we have  $\mathbb{E} \{ \mathbf{h}_k^* \mathbf{h}_k^T \} = \bar{\mathbf{h}}_k^* \bar{\mathbf{h}}_k^T$  and

$$\bar{\mathbf{h}}_k = \sqrt{\gamma_k} \mathbf{v}_k. \quad (9)$$

Note that the required sCSI knowledge involves the channel gain  $\gamma_k$  and the UPA response  $\mathbf{v}_k$ , which are regarded to be constant during the observed interval and can be updated dynamically in accordance with the channel variation [17]. Subsequently, the upper bound of the ergodic rate with the sCSI knowledge is given by

$$\bar{R}_k = \log \left( 1 + \frac{|\bar{\mathbf{h}}_k^T \mathbf{w}_k|^2}{\sum_{\ell \neq k} |\bar{\mathbf{h}}_k^T \mathbf{w}_\ell|^2 + N_0} \right), \quad (10)$$

where  $\bar{\mathbf{h}}_k$  is given in (9). The tightness of the upper bound has been established for the Rician channel assumption in [44], where the upper bound is proved to be even tighter with smaller transmission power and larger Rician factor. Besides, the tightness will also be verified by simulations in Section V. Finally, we can express the SE as<sup>7</sup>

$$\begin{aligned} R_{\text{sum}} &= \frac{1}{B_w} \sum_{k=1}^K \sum_{n=1}^{N_{\text{sc}}} f_s \bar{R}_{k,n} \\ &= \frac{1}{B_w} \sum_{k=1}^K \sum_{n=1}^{N_{\text{sc}}} f_s \log \left( 1 + \frac{|\bar{\mathbf{h}}_{k,n}^T \mathbf{w}_{k,n}|^2}{\sum_{\ell \neq k} |\bar{\mathbf{h}}_{k,n}^T \mathbf{w}_{\ell,n}|^2 + N_0} \right), \end{aligned} \quad (11)$$

where  $\bar{\mathbf{h}}_{k,n} = \sqrt{\gamma_{k,n}} \mathbf{v}_{k,n}$ .

## B. Localization Accuracy

1) *Received Signal Model*: The received pilot signal at the  $k$ th UT is given by<sup>8</sup>

$$y_{k,m,n} = \left( (\mathbf{h}_{k,m,n}^{\text{los}})^T + (\mathbf{h}_{k,m,n}^{\text{nlos}})^T \right) \mathbf{W}_n \mathbf{s}_{m,n} + z_{k,m,n}.$$

<sup>7</sup>For notation brevity, the OFDM symbol index  $m_d$  is omitted here as the following focus is on each time slot.

<sup>8</sup>The superscript and subscript  $p$  is omitted for notation brevity.

For notation convenience, we denote  $\tilde{z}_{k,m,n} = (\mathbf{h}_{k,m,n}^{\text{nlos}})^T \mathbf{W}_n \mathbf{s}_{m,n} + z_{k,m,n}$ , and then, (12) can be converted into  $y_{k,m,n} = (\mathbf{h}_{k,m,n}^{\text{los}})^T \mathbf{W}_n \mathbf{s}_{m,n} + \tilde{z}_{k,m,n}$ , where  $\tilde{z}_{k,m,n}$  follows  $\mathcal{CN}(0, N_{k,n}^{\text{eq}})$ , and the variance  $N_{k,n}^{\text{eq}}$  is given by  $N_{k,n}^{\text{eq}} = \mathbb{E} \{ |\tilde{z}_{k,m,n}|^2 \} = \frac{\gamma_k}{1+\kappa_k} \mathbf{v}_{k,n}^T \mathbf{W}_n \mathbf{W}_n^H \mathbf{v}_{k,n} + N_0$ .

2) *Fisher Information Matrix (FIM)*: As mentioned before, channel parameters can be estimated from the received signals. The corresponding channel parameters between the satellite and the  $k$ th UT can be characterized by a  $6 \times 1$  vector  $\boldsymbol{\eta}_k = [\theta_k^x, \theta_k^y, \tau_k, \nu_k, \alpha_k^R, \alpha_k^I]^T$ , where  $\alpha_k^R$  and  $\alpha_k^I$  are the real and imaginary parts of  $\alpha_k$ , respectively. Then, we denote  $\hat{\boldsymbol{\eta}}_k$  as an estimate for the parameter vector  $\boldsymbol{\eta}_k$  associated with the  $k$ th UT, the mean squared error (MSE) of which allows a lower bound, given by  $\mathbb{E} \{ (\hat{\boldsymbol{\eta}}_k - \boldsymbol{\eta}_k)(\hat{\boldsymbol{\eta}}_k - \boldsymbol{\eta}_k)^T \} \succeq \mathbf{J}_{\boldsymbol{\eta}_k}^{-1}$ . Note that  $\mathbf{J}_{\boldsymbol{\eta}_k}$  is the FIM for the unknown vector  $\boldsymbol{\eta}_k$  and the  $(i, j)$ th element can be computed from [19], [33], [45], [46]

$$\begin{aligned} [\mathbf{J}_{\boldsymbol{\eta}_k}]_{i,j} &= \sum_{m=1}^M \sum_{n=1}^{N_{\text{sc}}} [\mathbf{J}_{\boldsymbol{\eta}_k}]_{i,j}^{m,n} \\ &= \sum_{m=1}^M \sum_{n=1}^{N_{\text{sc}}} \frac{2}{N_{k,n}^{\text{eq}}} \Re \left\{ \mathbb{E} \left\{ \frac{\partial (r_{k,m,n})^H}{\partial [\boldsymbol{\eta}_k]_i} \frac{\partial r_{k,m,n}}{\partial [\boldsymbol{\eta}_k]_j} \right\} \right\}, \end{aligned} \quad (12)$$

where  $r_{k,m,n} = (\mathbf{h}_{k,m,n}^{\text{los}})^T \mathbf{W}_n \mathbf{s}_{m,n}$  is the received pilot signal excluding the noise.

3) *Transformation for Position Parameters*: Note that the transformation from channel parameters  $\boldsymbol{\eta}_k$  to  $\bar{\boldsymbol{\eta}}_k = [\mathbf{p}_k^T, \alpha_k^R, \alpha_k^I]^T$  is a bijection. Then, the transformed FIM involved the position information associated with the  $k$ th UT is given by  $\mathbf{J}_{\bar{\boldsymbol{\eta}}_k} = \boldsymbol{\Gamma}_k \mathbf{J}_{\boldsymbol{\eta}_k} \boldsymbol{\Gamma}_k^T$ . The transformation matrix  $\boldsymbol{\Gamma}_k \in \mathbb{R}^{5 \times 6}$  is given by

$$\boldsymbol{\Gamma}_k \triangleq \frac{\partial \boldsymbol{\eta}_k^T}{\partial \bar{\boldsymbol{\eta}}_k} = \text{blkdiag} \{ \boldsymbol{\Xi}_k, \mathbf{I}_2 \}, \quad (13)$$

where  $\boldsymbol{\Xi}_k$  is detailed in Appendix A.

4) *SPEB*: Localization precision can be measured by the metric squared position error (SPE), the definition of which is the MSE between the actual position  $\mathbf{p}_k$  of the  $k$ th UT and its estimation  $\hat{\mathbf{p}}_k$  [7], i.e.,  $\rho_k(\mathbf{W}) = \mathbb{E} \{ \|\hat{\mathbf{p}}_k - \mathbf{p}_k\|_2^2 \}$ . Following the information inequality, the bound of the SPE is given by  $\rho_k(\mathbf{W}) \geq \text{Tr} \{ (\mathbf{J}_{\mathbf{p}_k}^{\text{e}})^{-1} \}$  [29]. Then, we define the sum SPEB of the UTs as

$$\rho_{\text{sum}}^{\text{b}} = \sum_{k=1}^K \text{Tr} \{ [\mathbf{J}_{\bar{\boldsymbol{\eta}}_k}^{-1}]_{1:3,1:3} \} = \sum_{k=1}^K \text{Tr} \{ \mathbf{E}^T \mathbf{J}_{\bar{\boldsymbol{\eta}}_k}^{-1} \mathbf{E} \}. \quad (14)$$

where  $\mathbf{E} = [\mathbf{e}_1, \mathbf{e}_2, \mathbf{e}_3]$ , and  $\mathbf{e}_i \in \mathbb{R}^{5 \times 1}$  denotes a vector with the  $i$ th element being one while the others being zero.

## IV. INTEGRATED COMMUNICATIONS AND LOCALIZATION

### A. Problem Formulation

Our work aims to design a hybrid precoding approach for the considered LEO satellite ICAL systems. To that end, an optimization problem is formulated, to maximize the downlink SE<sup>9</sup> and minimize the sum SPEB. Let  $\mathcal{W} = \{ \mathbf{W}_{\text{BB},n} \}_{n=1}^{N_{\text{sc}}}$ ,

<sup>9</sup>Here, we omit the constant  $f_s/B_w$  in the expression of the SE for brevity.

and we define a vector of the objectives as  $f(\mathcal{W}, \mathbf{W}_{\text{RF}}) = [R_{\text{sum}}, -\rho_{\text{sum}}^b]^T$ , then the multi-objective optimization problem is given by [47]

$$\mathcal{P}_1 : \underset{\mathcal{W}, \mathbf{W}_{\text{RF}}}{\text{maximize}} \quad f(\mathcal{W}, \mathbf{W}_{\text{RF}}) \quad (15a)$$

$$\text{s.t.} \quad \sum_{n=1}^{N_{\text{sc}}} \|\mathbf{W}_{\text{RF}} \mathbf{W}_{\text{BB},n}\|_F^2 \leq P, \quad (15b)$$

$$\mathbf{W}_{\text{RF}} \in \mathcal{S}. \quad (15c)$$

Note that problem  $\mathcal{P}_1$  is the maximization problem of the vector  $f(\mathcal{W}, \mathbf{W}_{\text{RF}})$  with both communication and localization metrics, which is defined to simultaneously maximize those two elements [48]. In Eq. (15),  $P$  is the transmit power budget, and  $\mathcal{S} \in \{\mathcal{S}_{\text{FC}}, \mathcal{S}_{\text{PC}}\}$  for the fully and partially connected structures, respectively. For the partially connected structure, the antennas are divided into  $N_{\text{rf}}$  groups, where each group allows  $N_g = N_t/N_{\text{rf}}$  antenna elements. Thus, the corresponding analog precoding matrix is block diagonal, given by  $\mathbf{W}_{\text{RF}} = \text{blkdiag}\{\mathbf{w}_{\text{RF},1}, \dots, \mathbf{w}_{\text{RF},N_{\text{rf}}}\}$ . Besides, the communication and localization metric components of the objective in Eq. (15a) have different units, and thus, we respectively transform them into dimensionless ones in the first place [47]. Then, a weighted sum method is exploited for the problem with transformed objectives to trade-off between the performance of communications and localization, where a positive weighting coefficient is selected to satisfy the condition for Pareto optimality [47, Definition 1]. Note that several systematic techniques have been developed to determine the weighting coefficient, i.e., ranking methods [49] and eigenvalue method [50]. Finally, we jointly design the digital precoder for each subcarrier and the analog precoder for all subcarriers.

### B. Spectral Efficiency Maximization

For notation brevity, let the product of the hybrid precoders denoted by  $\mathbf{W}_n = \mathbf{W}_{\text{RF}} \mathbf{W}_{\text{BB},n}$ . By utilizing weighted minimum MSE (WMMSE) method, the maximization of SE can be equivalently transformed into minimizing the weighted sum MSE [51]. In particular, we assume that linear combiner  $u_{k,n}$  is incorporated at subcarrier  $n$  of the  $k$ th UT. Then, by letting  $\mathbf{U} = \{u_{k,n}\}_{k=1, n=1}^{K, N_{\text{sc}}}$  and introducing an auxiliary weight variable  $\Omega = \{\omega_{k,n}\}_{k=1, n=1}^{K, N_{\text{sc}}}$ , the weighted sum MSE is given by  $\varepsilon^{\text{sum}} = \sum_{k=1}^K \sum_{n=1}^{N_{\text{sc}}} \omega_{k,n} \varepsilon_{k,n}(\mathbf{W}_n, u_{k,n}) - \log(\omega_{k,n})$ , where  $\varepsilon_{k,n}(\mathbf{W}_n, u_{k,n})$  is the MSE between the estimated signal  $\hat{s}_{k,n} = u_{k,n}^* y_{k,n}$  and the transmitted signal  $s_{k,n}$ , given by

$$\begin{aligned} \varepsilon_{k,n}(\mathbf{W}_n, u_{k,n}) &= \mathbb{E} \left\{ (\hat{s}_{k,n} - s_{k,n}) (\hat{s}_{k,n} - s_{k,n})^H \right\} \\ &= |u_{k,n}^* \bar{\mathbf{h}}_{k,n}^T \mathbf{w}_{k,n} - 1|^2 + \sum_{i \neq k} |u_{k,n}^* \bar{\mathbf{h}}_{k,n}^T \mathbf{w}_{i,n}|^2 + N_0 |u_{k,n}|^2. \end{aligned} \quad (16)$$

Note that when the transmitter precoders are known, the minimum MSE (MMSE) receiver can be given by  $u_{k,n}^{\text{MMSE}} = \bar{\mathbf{h}}_{k,n}^T \mathbf{w}_{k,n} (\sum_{i=1}^K |\bar{\mathbf{h}}_{k,n}^T \mathbf{w}_{i,n}|^2 + N_0)^{-1}$ .

### C. Sum SPEB Minimization

Note that the sum SPEB component of the objective in Eq. (15a) is not easy to tackle due to the tightly coupled digital and analog precoding matrices. In this section, we regard the product of the digital and analog precoding matrices as a whole, i.e.,  $\mathbf{W}_n^{\text{loc}} = \mathbf{W}_{\text{RF}} \mathbf{W}_{\text{BB},n}$ ,  $\forall n$ , and our objective is to find the fully digital precoder  $\mathbf{W}_n^{\text{loc}}$  to minimize the sum SPEB, which can be formulated as

$$\mathcal{P}_2 : \underset{\{\mathbf{W}_n^{\text{loc}}\}_{n=1}^{N_{\text{sc}}}}{\text{minimize}} \quad \sum_{k=1}^K \text{Tr} \{ \mathbf{E}^T \mathbf{J}_{\bar{\eta}_k}^{-1} \mathbf{E} \} \quad \text{s.t.} \quad \sum_{n=1}^{N_{\text{sc}}} \|\mathbf{W}_n^{\text{loc}}\|_F^2 \leq P. \quad (17)$$

Note that problem  $\mathcal{P}_2$  has been investigated in the terrestrial systems, where the elements of FIM are linearly dependent on the optimization variable. However, for the LEO satellite scenarios, the linear dependence no longer exists, and problem  $\mathcal{P}_2$  requires transformation into a convex problem to be effectively addressed. The minimization of the sum SPEB is converted into minimizing the sum Euclidean distance between the product of the hybrid precoders and the precoders obtained from problem  $\mathcal{P}_2$ . Then, let  $\mathbf{C}_n \triangleq \mathbf{W}_n^{\text{loc}} (\mathbf{W}_n^{\text{loc}})^H$  and problem  $\mathcal{P}_2$  can be converted into a rank-constrained problem

$$\begin{aligned} \mathcal{P}_3 : \underset{\mathbf{C}_n}{\text{minimize}} \quad & \sum_{k=1}^K \text{Tr} \{ \mathbf{E}^T \mathbf{J}_{\bar{\eta}_k}^{-1} \mathbf{E} \} \\ \text{s.t.} \quad & \sum_{n=1}^{N_{\text{sc}}} \text{Tr} \{ \mathbf{C}_n \} \leq P, \quad \mathbf{C}_n \succeq \mathbf{0}, \quad \text{rank} \{ \mathbf{C}_n \} \leq K. \end{aligned} \quad (18a)$$

Then, we introduce an auxiliary variable  $\mathbf{M}_k \in \mathbb{R}^{3 \times 3}$ , which satisfies the following condition [52]

$$\mathbf{M}_k \succeq \mathbf{E}^T \mathbf{J}_{\bar{\eta}_k}^{-1} \mathbf{E}, \quad \forall k. \quad (19)$$

Note that the FIM  $\mathbf{J}_{\bar{\eta}_k}$  must be a positive semidefinite matrix, and thus, utilizing the property of Schur complement, Eq. (19) can be transformed into [52]

$$\begin{bmatrix} \mathbf{M}_k & \mathbf{E}^T \\ \mathbf{E} & \mathbf{J}_{\bar{\eta}_k}(\mathbf{C}_n) \end{bmatrix} \succeq \mathbf{0}, \quad \forall k. \quad (20)$$

Therefore, problem  $\mathcal{P}_3$  can be converted into [52], [53]

$$\mathcal{P}_4 : \underset{\mathbf{C}_n, \mathbf{M}_k}{\text{minimize}} \quad \sum_{k=1}^K \text{Tr} \{ \mathbf{M}_k \} \quad (21a)$$

$$\text{s.t.} \quad \sum_{n=1}^{N_{\text{sc}}} \text{Tr} \{ \mathbf{C}_n \} \leq P, \quad (21b)$$

$$\mathbf{C}_n \succeq \mathbf{0}, \quad (21c)$$

$$\text{rank} \{ \mathbf{C}_n \} \leq K, \quad (21d)$$

$$\begin{bmatrix} \mathbf{M}_k & \mathbf{E}^T \\ \mathbf{E} & \mathbf{J}_{\bar{\eta}_k}(\mathbf{C}_n) \end{bmatrix} \succeq \mathbf{0}, \quad \forall k. \quad (21e)$$

Note that the rank constraint in (21d) of problem  $\mathcal{P}_4$  is difficult to handle. Therefore, we first focus on the relaxed problem by dropping this rank constraint [54]. To further improve computational efficiency, based on [55, Appendix C], the relaxed problem of  $\mathcal{P}_4$  allows a optimal solution, which is

given by

$$\mathbf{C}_n = \mathbf{L}_n \mathbf{Z}_n \mathbf{L}_n^H. \quad (22)$$

The proof is given in Appendix B. In Eq. (22),  $\mathbf{Z}_n$  denotes a  $3K \times 3K$ -dimensional positive semidefinite matrix and  $\mathbf{L}_n = [\mathbf{V}_n \ \mathbf{V}_{n,x} \ \mathbf{V}_{n,y}]$ , where  $\mathbf{V}_n = [\mathbf{v}_{1,n}, \dots, \mathbf{v}_{K,n}]$ ,  $\mathbf{V}_{n,d} = [\mathbf{v}_{1,n,\theta_1^d}, \dots, \mathbf{v}_{K,n,\theta_K^d}]$ , and  $\mathbf{v}_{k,n,\theta_1^d} \triangleq \partial \mathbf{v}_{k,n} / \partial \theta_1^d$  for  $d \in \{x, y\}$ . By utilizing the decomposition in Eq. (22), problem  $\mathcal{P}_4$  can be converted into

$$\mathcal{P}_5 : \underset{\mathbf{Z}_n, \mathbf{M}_k}{\text{minimize}} \sum_{k=1}^K \text{Tr} \{ \mathbf{M}_k \} \quad (23a)$$

$$\text{s.t.} \sum_{n=1}^{N_{\text{sc}}} \text{Tr} \{ \mathbf{L}_n \mathbf{Z}_n \mathbf{L}_n^H \} \leq P, \quad (23b)$$

$$\mathbf{Z}_n \succeq \mathbf{0}, \quad (23c)$$

$$\begin{bmatrix} \mathbf{M}_k & \mathbf{E}^T \\ \mathbf{E} & \mathbf{J}_{\hat{\eta}_k}(\mathbf{Z}_n) \end{bmatrix} \succeq \mathbf{0}, \quad \forall k. \quad (23d)$$

To tackle problem  $\mathcal{P}_5$ , since  $\mathbf{J}_{\hat{\eta}_k}(\mathbf{Z}_n)$  is not convex with respect to the variable  $\mathbf{Z}_n$ , we invoke the majorization-minimization (MM) algorithm, the basic philosophy of which is to iteratively handle problem  $\mathcal{P}_5$  through a series of easier problems [56]. In particular, let  $\mathbf{Z}_{n,t}$  denote the solution of the  $t$ th iteration, and then, in  $(t+1)$ th iteration, we substitute  $\mathbf{J}_{\hat{\eta}_k}(\mathbf{Z}_n)$  with its second order Taylor expansion  $\hat{\mathbf{J}}_{\hat{\eta}_k}(\mathbf{Z}_n)$ , whose  $(i, j)$ th element is given in (24) on the top of the next page. In (24), the first order gradient of  $[\mathbf{J}_{\hat{\eta}_k}]_{i,j}^{m,n}(\mathbf{Z}_{n,t})$  with respect to the variable  $\mathbf{Z}_{n,t}$  is given in (25) on the top of the next page, where  $\mathbf{A}_{k,m,n,i,j} = \mathbf{L}_n^H \frac{\partial \mathbf{h}_{k,m,n}^*}{\partial [\eta_k]_i} \frac{\partial \mathbf{h}_{k,m,n}^T}{\partial [\eta_k]_j} \mathbf{L}_n$  and  $\mathbf{D}_{k,n} = \frac{\gamma_k}{1+\kappa_k} \mathbf{L}_n^H \mathbf{v}_{k,n}^* \mathbf{v}_{k,n}^T \mathbf{L}_n$ .

Then, in the  $(t+1)$ th iteration, the corresponding problem can be written as

$$\mathcal{P}_5^{(t+1)} : \underset{\mathbf{Z}_{n,t+1}, \mathbf{M}_{k,t+1}}{\text{minimize}} \sum_{k=1}^K \text{Tr} \{ \mathbf{M}_{k,t+1} \} \quad (26a)$$

$$\text{s.t.} \sum_{n=1}^{N_{\text{sc}}} \text{Tr} \{ \mathbf{L}_n \mathbf{Z}_{n,t+1} \mathbf{L}_n^H \} \leq P, \quad (26b)$$

$$\mathbf{Z}_{n,t+1} \succeq \mathbf{0}, \quad (26c)$$

$$\begin{bmatrix} \mathbf{M}_k & \mathbf{E}^T \\ \mathbf{E} & \hat{\mathbf{J}}_{\hat{\eta}_k}(\mathbf{Z}_{n,t+1}) \end{bmatrix} \succeq \mathbf{0}, \quad \forall k, \quad (26d)$$

which can be handled with semidefinite programming (SDP) solvers [57], [58]. Note that since the MM method results in a relaxed problem, each stationary point of the series involving the objective values produced by problem  $\mathcal{P}_5^{(t+1)}$  might be a local sub-optimum of problem  $\mathcal{P}_5$  [59]. Then, with the symmetric positive definite matrix  $\mathbf{Z}_n$  from  $\mathcal{P}_5$ , we have  $\mathbf{C}_n = \mathbf{L}_n \mathbf{Z}_n \mathbf{L}_n^H$ , and the corresponding localization precoder can be reversed through Cholesky decomposition and randomization procedures [35], [60]–[62].

*Remark 1:* Due to the roughness of the prior knowledge obtained at the LEO satellite side for the  $k$ th UT, robust signal design should be formulated with the consideration of the uncertainties in channel parameters, which can be performed

by referring to [35], [53].

#### D. Hybrid Precoding for the ICAL Systems

Let  $\bar{\mathbf{W}}_{\text{BB}} = [\mathbf{W}_{\text{BB},1}, \dots, \mathbf{W}_{\text{BB},N_{\text{sc}}}] \in \mathbb{C}^{N_{\text{rf}} \times K N_{\text{sc}}}$  and  $\bar{\mathbf{W}}^{\text{loc}} = [\mathbf{W}_1^{\text{loc}}, \dots, \mathbf{W}_{N_{\text{sc}}}^{\text{loc}}] \in \mathbb{C}^{N_{\text{t}} \times N_{\text{rf}} N_{\text{sc}}}$  for notation brevity. To design the digital and analog precoders, the following weighted sum problem is formulated to minimize the sum MSE of communications and the sum Euclidean distance between the hybrid precoders and the localization-only fully digital precoders, as obtained in Section IV-B and Section IV-C, which is given by [21], [63], [64]

$$\begin{aligned} \mathcal{Q}_1 : \underset{\mathbf{W}_{\text{RF}}, \{\mathbf{W}_{\text{BB},n}\}_{n=1}^{N_{\text{sc}}}, \mathbf{U}, \Omega}{\text{minimize}} \quad & \rho \varepsilon^{\text{sum}}(\mathbf{W}_{\text{RF}}, \bar{\mathbf{W}}_{\text{BB}}, \mathbf{U}, \Omega) \\ & + (1-\rho) d^{\text{sum}}(\mathbf{W}_{\text{RF}}, \bar{\mathbf{W}}_{\text{BB}}) \quad (27a) \\ \text{s.t.} \quad & \|\mathbf{W}_{\text{RF}} \bar{\mathbf{W}}_{\text{BB}}\|_F^2 \leq P, \quad \mathbf{W}_{\text{RF}} \in \mathcal{S}. \quad (27b) \end{aligned}$$

In (27),  $\rho \in [0, 1]$  denotes the weighting coefficient, serving to trade off between the performance of the communications and localization, and  $d^{\text{sum}}$  is defined as  $d^{\text{sum}}(\mathbf{W}_{\text{RF}}, \bar{\mathbf{W}}_{\text{BB}}) = \sum_{n=1}^{N_{\text{sc}}} \|\mathbf{W}_{\text{RF}} \mathbf{W}_{\text{BB},n} - \mathbf{W}_n^{\text{loc}}\|_F^2$ . By introducing the auxiliary variables  $\mathbf{G}_{k,n} = [\mathbf{g}_{k,n}^1, \dots, \mathbf{g}_{k,n}^K] = \mathbf{W}_{\text{RF}} \mathbf{W}_{\text{BB},n}$ ,  $\forall k$ , problem  $\mathcal{Q}_1$  can be reformulated as [64]

$$\begin{aligned} \mathcal{Q}_2 : \underset{\mathbf{W}_{\text{RF}}, \{\mathbf{W}_{\text{BB},n}\}_{n=1}^{N_{\text{sc}}}, \mathbf{U}, \Omega}{\text{minimize}} \quad & \sum_{k=1}^K \sum_{n=1}^{N_{\text{sc}}} \left[ \rho \varepsilon_{k,n}^{\text{w}}(\mathbf{G}_{k,n}, u_{k,n}, \omega_{k,n}) \right. \\ & \left. + \frac{1-\rho}{K} d_{k,n}(\mathbf{G}_{k,n}) \right] \quad (28a) \end{aligned}$$

$$\text{s.t.} \quad \mathbf{G}_{k,n} = \mathbf{W}_{\text{RF}} \mathbf{W}_{\text{BB},n}, \quad \forall k, \quad (28b)$$

$$\begin{aligned} & \sum_{k=1}^K \sum_{n=1}^{N_{\text{sc}}} \text{Tr} \{ \mathbf{G}_{k,n} \mathbf{G}_{k,n}^H \} \leq PK, \\ & \mathbf{W}_{\text{RF}} \in \mathcal{S}, \quad (28c) \end{aligned}$$

where  $\varepsilon_{k,n}^{\text{w}}(\mathbf{G}_{k,n}, u_{k,n}, \omega_{k,n}) = \omega_{k,n} \varepsilon_{k,n}(\mathbf{G}_{k,n}, u_{k,n}) - \log(\omega_{k,n})$ ,  $d_{k,n} = \|\mathbf{G}_{k,n} - \mathbf{W}_n^{\text{loc}}\|_F^2$  and  $\varepsilon_{k,n}(\mathbf{G}_{k,n}, u_{k,n}) = |u_{k,n}|^2 \mathbf{h}_{k,n}^T \mathbf{G}_{k,n} \mathbf{G}_{k,n}^H \mathbf{h}_{k,n}^* - u_{k,n} \mathbf{h}_{k,n}^T \mathbf{G}_{k,n} \mathbf{e}_k - u_{k,n}^* \mathbf{G}_{k,n}^H \mathbf{h}_{k,n}^* \mathbf{e}_k^T + 1 + N_0 |u_{k,n}|^2$ .

In the following, inspired by the alternating direction method of multipliers (ADMM) [65], we adopt the augmented Lagrangian method by introducing dual variables  $\mathbf{Q}_{k,n} \in \mathbb{C}^{N_{\text{t}} \times K}$ , and the corresponding penalty  $\eta_{k,n} > 0$ . Then, let  $\mathcal{G} = \{\mathbf{G}_{k,n}\}_{k=1,n=1}^{K,N_{\text{sc}}}$ ,  $\mathcal{Q} = \{\mathbf{Q}_{k,n}\}_{k=1,n=1}^{K,N_{\text{sc}}}$  and the objective of problem  $\mathcal{Q}_2$  can be transformed into

$$\begin{aligned} & f(\mathcal{G}, \mathbf{U}, \Omega, \bar{\mathbf{W}}_{\text{BB}}, \mathbf{W}_{\text{RF}}, \mathcal{Q}) \\ & = \sum_{k=1}^K \sum_{n=1}^{N_{\text{sc}}} L(\mathbf{G}_{k,n}, u_{k,n}, \omega_{k,n}, \mathbf{W}_{\text{BB},n}, \mathbf{W}_{\text{RF}}, \mathbf{Q}_{k,n}), \quad (29) \end{aligned}$$

where  $L(\mathbf{G}_{k,n}, u_{k,n}, \omega_{k,n}, \mathbf{W}_{\text{BB},n}, \mathbf{W}_{\text{RF}}, \mathbf{Q}_{k,n}) = \rho \varepsilon_{k,n}^{\text{w}}(\mathbf{G}_{k,n}, u_{k,n}, \omega_{k,n}, \mathbf{Q}_{k,n}) + \frac{1-\rho}{K} d_{k,n}(\mathbf{G}_{k,n}) + \frac{\eta_{k,n}}{2} \|\mathbf{G}_{k,n} - \mathbf{W}_{\text{RF}} \mathbf{W}_{\text{BB},n} + \mathbf{Q}_{k,n}\|_F^2$ . The corresponding problem  $\mathcal{Q}_3$  can be then written as

$$\mathcal{Q}_3 : \underset{\mathcal{G}, \mathbf{U}, \Omega, \bar{\mathbf{W}}_{\text{BB}}, \mathbf{W}_{\text{RF}}, \mathcal{Q}}{\text{minimize}} \quad f(\mathcal{G}, \mathbf{U}, \Omega, \bar{\mathbf{W}}_{\text{BB}}, \mathbf{W}_{\text{RF}}, \mathcal{Q}) \quad (30a)$$



$$\left[ \hat{\mathbf{J}}_{\bar{\eta}_k} \right]_{i,j}(\mathbf{Z}_n) = [\mathbf{J}_{\bar{\eta}_k}]_{i,j}(\mathbf{Z}_{n,t}) + \sum_{m=1}^M \sum_{n=1}^{N_{\text{sc}}} \text{Tr} \left\{ \left( \frac{\partial [\mathbf{J}_{\bar{\eta}_k}]_{i,j}^{m,n}(\mathbf{Z}_{n,t})}{\partial \mathbf{Z}_{n,t}} \right)^T (\mathbf{Z}_n - \mathbf{Z}_{n,t}) \right\} + \frac{L}{2} \|\mathbf{Z}_n - \mathbf{Z}_{n,t}\|_F^2 \quad (24)$$

$$\frac{\partial [\mathbf{J}_{\bar{\eta}_k}]_{i,j}^{m,n}(\mathbf{Z}_{n,t})}{\partial \mathbf{Z}_{n,t}} = \frac{(\text{Tr}\{\mathbf{D}_{k,n}\mathbf{Z}_{n,t}\} + N_0) \mathbf{A}_{k,m,n,i,j} - \text{Tr}\{\mathbf{Z}_{n,t}\mathbf{A}_{k,m,n,i,j}\} \cdot \mathbf{D}_{k,n}}{(\text{Tr}\{\mathbf{D}_{k,n}\mathbf{Z}_{n,t}\} + N_0)^2} \quad (25)$$

$$\text{s.t.} \quad \sum_{k=1}^K \sum_{n=1}^{N_{\text{sc}}} \text{Tr}\{\mathbf{G}_{k,n} \mathbf{G}_{k,n}^H\} \leq PK, \quad (30b)$$

$$\mathbf{W}_{\text{RF}} \in \mathcal{S}, \quad (30c)$$

which can be handled through the ADMM method [65]. In each iteration of the ADMM method, the algorithmic steps mainly depend on the optimization of each variable in problem  $\mathcal{Q}_3$ . It is worth noting that, in each iteration, the architecture of the ADMM allows us to update variables  $\mathbf{G}_{k,n}$ ,  $u_{k,n}$ ,  $\omega_{k,n}$ , and  $\mathbf{W}_{\text{BB},n}$  in parallel [66]. Then, the corresponding steps for handling problem  $\mathcal{Q}_3$  by the ADMM are given by

$$\mathcal{G}^t \leftarrow \arg \min_{(30b)} f(\mathcal{G}, \mathbf{U}^{t-1}, \mathbf{\Omega}^{t-1}, \bar{\mathbf{W}}_{\text{BB}}^{t-1}, \mathbf{W}_{\text{RF}}^{t-1}, \mathcal{Q}^{t-1}), \quad (31)$$

$$\mathbf{U}^t \leftarrow \arg \min f(\mathcal{G}^t, \mathbf{U}, \mathbf{\Omega}^{t-1}, \bar{\mathbf{W}}_{\text{BB}}^{t-1}, \mathbf{W}_{\text{RF}}^{t-1}, \mathcal{Q}^{t-1}), \quad (32)$$

$$\mathbf{\Omega}^t \leftarrow \arg \min f(\mathcal{G}^t, \mathbf{U}^t, \mathbf{\Omega}, \bar{\mathbf{W}}_{\text{BB}}^{t-1}, \mathbf{W}_{\text{RF}}^{t-1}, \mathcal{Q}^{t-1}), \quad (33)$$

$$\bar{\mathbf{W}}_{\text{BB}}^t \leftarrow \arg \min f(\mathcal{G}^t, \mathbf{U}^t, \mathbf{\Omega}^t, \bar{\mathbf{W}}_{\text{BB}}, \mathbf{W}_{\text{RF}}^{t-1}, \mathcal{Q}^{t-1}), \quad (34)$$

$$\mathbf{W}_{\text{RF}}^t \leftarrow \arg \min_{(30c)} f(\mathcal{G}^t, \mathbf{U}^t, \mathbf{\Omega}^t, \bar{\mathbf{W}}_{\text{BB}}^t, \mathbf{W}_{\text{RF}}, \mathcal{Q}^{t-1}), \quad (35)$$

$$\mathbf{Q}_{k,n}^t \leftarrow \mathbf{Q}_{k,n}^{t-1} + \mathbf{G}_{k,n}^t - \mathbf{W}_{\text{RF}}^t \mathbf{W}_{\text{BB},n}^t, \quad (36)$$

the solution of which is detailed in Appendix C. To further improve the convergence rate, at the end of each iteration, the penalty  $\eta_{k,n}$  is updated according to [65, Eq. (3.13)]

$$\eta_{k,n}^{t+1} = \begin{cases} \zeta^{\text{mul}} \eta_{k,n}^t, & \frac{\|\mathbf{G}_{k,n}^{t+1} - \mathbf{W}_{\text{RF}}^{t+1} \mathbf{W}_{\text{BB},n}^{t+1}\|_F^2}{\|\mathbf{G}_{k,n}^{t+1} - \mathbf{G}_{k,n}^t\|_F^2} > \varrho, \\ \eta_{k,n}^t / \zeta^{\text{div}}, & \frac{\|\mathbf{G}_{k,n}^{t+1} - \mathbf{W}_{\text{RF}}^{t+1} \mathbf{W}_{\text{BB},n}^{t+1}\|_F^2}{\|\mathbf{G}_{k,n}^{t+1} - \mathbf{G}_{k,n}^t\|_F^2} < 1/\varrho, \\ \eta_{k,n}^t, & \text{otherwise,} \end{cases} \quad (37)$$

where  $\varrho > 1$  and  $\zeta^{\text{mul}}, \zeta^{\text{div}} > 1$ . The whole procedure for computing the hybrid precoders for LEO satellite ICAL is summarized in **Algorithm 1**.

### E. Convergence and Computational Complexity

The convergence of **Algorithm 1** depends on two parts. First, the sum SPEB minimization problem is handled with MM method by transforming the projection matrices, i.e.,  $\text{Tr}\{\mathbf{E}^T \mathbf{J}_{\bar{\eta}_k}^{-1} \mathbf{E}\}$ , with their second-order Taylor expansion, and according to [56], the sequence of feasible points  $\{\mathbf{Z}_{n,t}\}$  can converge to a stationary value. According to [67], the ADMM algorithm is guaranteed to be convergent to a stationary point when the penalty is properly chosen.

---

### Algorithm 1 Hybrid Precoding for ICAL

---

**Input:** Thresholds  $\epsilon_1, \epsilon_2 > 0$ .

**Output:** Hybrid precoders  $\mathbf{W}_{\text{RF}}$  and  $\mathbf{W}_{\text{BB},n}$ ,  $n = 1, \dots, N_{\text{sc}}$ .

- 1: Initialize  $t = 0$ ,  $t_{\text{max}}^{\text{loc}}$  and  $\mathbf{Z}_{n,t}$  such that  $\|\mathbf{L}_n \mathbf{Z}_{n,t} \mathbf{L}_n\|_F^2 = P/N_{\text{sc}}$ .
  - 2: **repeat**
  - 3:   Solve SDP problem  $\mathcal{P}_8^{(t+1)}$  and obtain  $\mathbf{M}_{k,t+1}$ ,  $\mathbf{Z}_{n,t+1}$ .
  - 4:    $t = t + 1$ .
  - 5: **until**  $\left| \sum_{k=1}^K \text{Tr}\{\mathbf{M}_{k,t}\} - \sum_{k=1}^K \text{Tr}\{\mathbf{M}_{k,t-1}\} \right| > \epsilon_1$  or  $t \geq t_{\text{max}}^{\text{loc}}$ .
  - 6: Obtain  $\mathbf{C}_n = \mathbf{L}_n \mathbf{Z}_n \mathbf{L}_n^H$  and  $\mathbf{W}_n^{\text{loc}}$  by eigenvalue decomposing  $\mathbf{C}_n$ ,  $n = 1, \dots, N_{\text{sc}}$ .
  - 7: Initialize  $t = 0$ ,  $\mathcal{G}^t$ ,  $\mathbf{U}^t$ ,  $\mathbf{\Omega}^t$ ,  $\bar{\mathbf{W}}_{\text{BB}}^t$ ,  $\mathbf{W}_{\text{RF}}^t$ ,  $\mathcal{Q}^t$ ,  $t_{\text{max}}^{\text{hy}}$ .
  - 8: **while**  $\sum_{k=1}^K \sum_{n=1}^{N_{\text{sc}}} \|\mathbf{G}_{k,n}^t - \mathbf{W}_{\text{RF}}^t \mathbf{W}_{\text{BB},n}^t\|_F^2 > \epsilon_2$  or  $t \leq t_{\text{max}}^{\text{hy}}$  **do**
  - 9:    $t = t + 1$ .
  - 10:   Update  $\mathcal{G}^t$ ,  $\mathbf{U}^t$ ,  $\mathbf{\Omega}^t$ ,  $\bar{\mathbf{W}}_{\text{BB}}^t$ ,  $\mathbf{W}_{\text{RF}}^t$ ,  $\mathbf{Q}_{k,n}^t$  and  $\eta_{k,n}^t$  following Eqs. (31) – (37).
  - 11: **end while**
- 

The complexity of **Algorithm 1** is detailed as follows. First, in each iteration of the MM algorithm, the number of the optimized variables for the SDP in (26) is denoted by  $n_{\text{var}} = 9K^2 N_{\text{sc}} + 9K$ . The number of linear matrix inequality (LMI) constraints is  $M_{\text{LMI}} = K + N_{\text{sc}}$ , contributed by (26c) and (26d), respectively. Besides, the number of the rows or columns for the matrix of the  $i$ th LMI constraint is given by  $m_i = 9$ ,  $1 \leq i \leq K$  and  $m_i = 3K$ ,  $K + 1 \leq i \leq M_{\text{LMI}}$ . Thus, the complexity of the SDP in (26) is given by  $\mathcal{O}(n_{\text{var}}^2 \sum_{i=1}^{M_{\text{LMI}}} m_i^2 + n_{\text{var}} \sum_{i=1}^{M_{\text{LMI}}} m_i^3)$  [53]. By assuming the MM algorithm terminates in  $J_{\text{mm}}$  iterations, the overall complexity to handle problem  $\mathcal{P}_5$  can be evaluated as  $\mathcal{O}(J_{\text{mm}}(n_{\text{var}}^2 \sum_{i=1}^{M_{\text{LMI}}} m_i^2 + n_{\text{var}} \sum_{i=1}^{M_{\text{LMI}}} m_i^3))$ . The computational complexity of the eigenvalue decomposition for  $\mathbf{C}_n$ ,  $n = 1, \dots, N_{\text{sc}}$  is given by  $\mathcal{O}(N_{\text{sc}} N_t^3)$ . Subsequently, in each iteration of the ADMM, the corresponding parameters should be updated according to Eqs. (31) – (37), and the major computational complexity lies in the update of  $\mathbf{G}_{k,n}$ . In particular, the update for  $\mathbf{G}_{k,n}$  in step Eq. (31) mainly contributes to the pseudo-inverse operation and the eigenvalue decomposition, both of which present the complexity of  $\mathcal{O}(N_t^3)$ . The computation of  $u_{k,n}$  and  $\omega_{k,n}$  in Eqs. (32) and (33) mainly depends on the multiplication operation  $\mathbf{h}_{k,n}^T \mathbf{G}_{k,n}$ , which requires the complexity of  $\mathcal{O}(N_t K)$ . Besides, both updates



for the baseband precoder  $\mathbf{W}_{\text{BB},n}$  and the analog precoder  $\mathbf{W}_{\text{rf}}$  in Eqs. (34) and (35) contributes  $\mathcal{O}(N_{\text{rf}}^3)$  to the algorithm's complexity. In addition, the computational complexity of both Eqs. (36) and (37) results from the multiplication of  $\mathbf{W}_{\text{RF}}$  and  $\mathbf{W}_{\text{BB},n}$ , which can be evaluated as  $\mathcal{O}(N_{\text{t}}N_{\text{rf}}K)$ . Then, assuming the ADMM algorithm terminates in  $J_{\text{admm}}$  iterations, the complexity for the ADMM can be estimated as  $\mathcal{O}(2J_{\text{admm}}KN_{\text{sc}}N_{\text{t}}^3)$ .

## V. SIMULATIONS

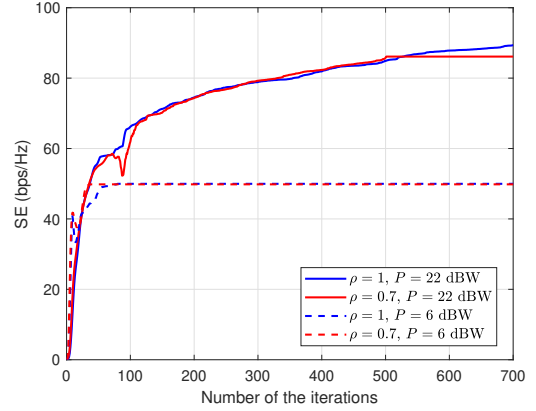
In this section, we evaluate the communication and localization performance for the proposed massive MIMO LEO satellite ICAL system, which is assumed to operate in the S-band. The performance of the communications and localization is evaluated with the downlink SE and average position error bound (APEB), which is defined as  $\rho_{\text{avg}}^{\text{b}} = \sqrt{\rho_{\text{sum}}^{\text{b}}/K}$ , respectively. Some related typical simulation parameters are given in Table I [68], [69]. The LEO satellite is assumed to be located at  $\mathbf{q} = [0, 0, 0]^T$  and the orientation angle is given by  $\mathbf{o} = [0, 0]^T$ . The maximum nadir angle of the UT is set to be  $\vartheta_{\text{max}} = \pi/6$  and each component of the AoD pair for the UT, i.e.,  $\theta_k^x$  and  $\theta_k^y$ , is assumed to be uniformly distributed in  $[\pi/2 - \vartheta_{\text{max}}, \pi/2 + \vartheta_{\text{max}}]$ . The nadir angle of the  $k$ th UT can be calculated as  $\vartheta_k = \arccos(\sin \theta_k^x \sin \theta_k^y)$  and thus, the elevation angle for the  $k$ th UT is given by  $\varphi_k = \arccos\left(\frac{R_e + H}{R_e} \sin \vartheta_k\right)$ , where  $R_e$  is the earth radius and  $H$  is the orbit height of the LEO satellite [24], [70]. Then, the distance between the LEO satellite and the  $k$ th UT can be calculated as  $d_k = \sqrt{H^2 + 2HR_e + R_e^2 \sin^2 \varphi_k} - R_e \sin \varphi_k$ . The channel gain  $\gamma_k$  is defined as

$$\gamma_k = G_{\text{sat}}G_{\text{ut}}N_{\text{t}}\left(\frac{c}{4\pi f_c d_k}\right)^2, \quad (38)$$

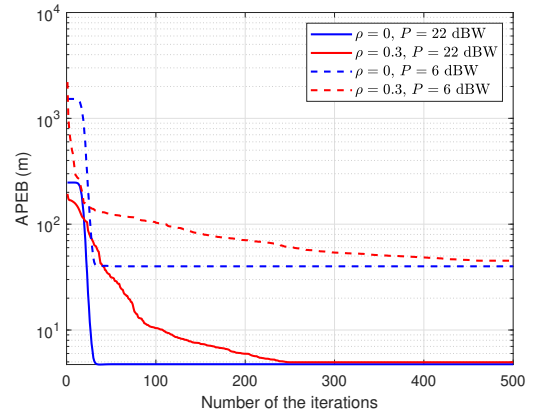
where  $G_{\text{sat}}$  and  $G_{\text{ut}}$  denote the antenna gain at the satellite and the UTs, respectively. The velocity of each UT at x, y, or z-axis is assumed to be uniformly distributed in  $[-10, 10]$  m/s.

Fig. 4 presents the values of the SE and APEB versus the number of iterations under different transmit power budgets with different weighting coefficients for **Algorithm 1**. In general, as the number of iterations increases, the performance of both communications and localization tends to be better. Then, as depicted in Fig. 4, the proposed method can converge to certain points for typical scenarios.

Fig. 5 illustrates the relationship between the transmit power and the SE as well as the APEB. As observed from Fig. 5(a), the tightness of the upper bound in Eq. (10) is verified. It is worth noting that  $\rho = 1$  and  $\rho = 0$  refer to the pure communication and pure localization system, respectively. The proposed ICAL system outperforms the pure communication and pure localization ones in APEB and SE, respectively. Besides, with larger transmit power, the SE sees an increase, and the APEB decreases, leading to better performance of both communications and localization. Under the scenario that a weighting coefficient  $\rho = 0.7$  is allocated for communications, both the SE and APEB can be enhanced, especially with higher transmit power. With a smaller weighting coefficient, i.e.,



(a) SE.



(b) APEB.

Fig. 4. The SE and APEB versus the number of iterations.

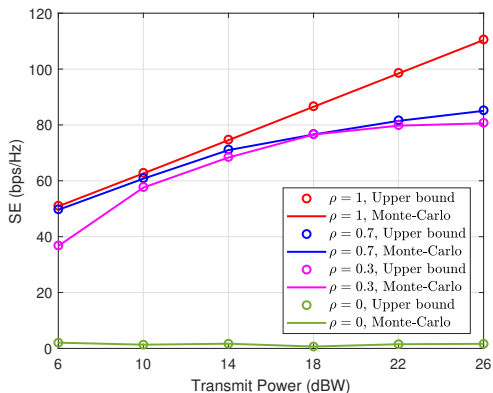
$\rho = 0.3$ , the ICAL system presents better APEB performance at the cost of the SE performance, compared with the case when  $\rho = 0.3$ . Moreover, Fig. 6 demonstrates the trade-off between communication SE and localization APEB for different transmit power. Besides, several typical values of the weighting coefficient are considered for their influence on both SE and APEB. In particular, larger weighting coefficient refers to the scenario that lies emphasis on communications, and thus, as observed, with the same APEB, larger weighting coefficient leads to better SE performance. The above analysis naturally leads to a conclusion that the proposed ICAL system can offer satisfying communication and localization performance, thanks to the high angular resolution brought by massive MIMO.

Fig. 7 compares the SE and APEB performance with different precoding design strategies as follows:

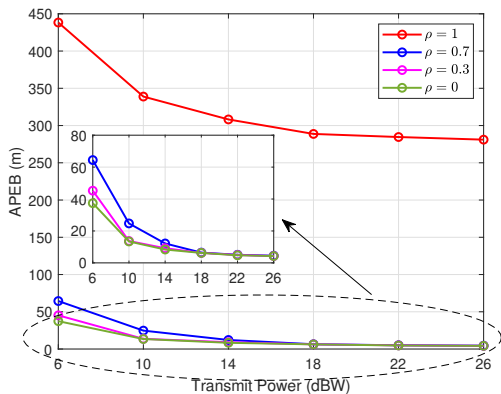
- The hybrid precoders with  $N_{\text{rf}}$  RF chains under both fully and partially connected structures for different weighting coefficients, as discussed in Section IV-A.
- The optimized fully digital precoder with  $N_{\text{t}}$  RF chains, i.e., the hybrid precoder with  $\mathbf{W}_{\text{RF}} = \mathbf{I}_{N_{\text{t}}}$  and  $\mathbf{W}_{\text{BB},n}$  optimized only [8].
- The standard directional beam codebook-based precoder with  $N_{\text{t}}$  RF chains, i.e.,

TABLE I  
SIMULATION PARAMETERS

Parameter	Value
System bandwidth $B_w$	15.36 MHz
Carrier frequency $f_c$	2 GHz
Speed of light $c$	$3 \times 10^8$ m/s
Carrier wavelength $\lambda_c$	0.15 m
Subcarrier separation $f_s$	30 kHz
Channel	
Number of valid subcarriers $N_{sc}$	512
Sampling rate $1/T_s$	30.72 MHz
Number of slots per frame $M_s$	20
Number of CP $N_{cp}$	36
Rician factor $\kappa_k$	18 dB
Number of OFDM symbols per slot $M_{sp}, M_{sd}$	2, 12
Satellite	
Orbit height $H$	200 km
Number of antennas $N_t$	$24 \times 24$
Antenna spacing $r_x, r_y$	$\lambda_c/2$
Number of RF chains $N_{rf}$	36
Antenna gain $G_{sat}, G_{ut}$	6 dB, 0 dB
UTs	
Number of UTs $K$	9
Noise spectral density	-174 dBm/Hz



(a) SE.



(b) APEB.

Fig. 5. SE and APEB performance versus transmit power  $P$  with  $N_t = 576$  antennas under the fully connected structure for different weighting coefficients  $\rho$ .

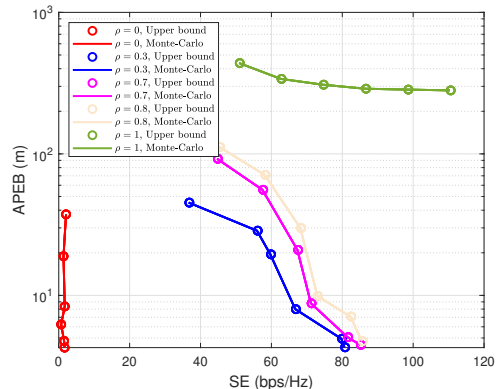


Fig. 6. Trade-off between communication SE and localization APEB for different transmit power under typical values of the weighting coefficient.

$$\mathbf{W}_n = \sqrt{P/K/N_{sc}} [\mathbf{v}_{1,n}^*, \dots, \mathbf{v}_{K,n}^*] \quad [53].$$

As observed from Fig. 7, for pure communications and localization, the hybrid scheme with the fully connected structure presents comparable performance with the fully digital scheme with fewer RF chains and thus, less static power consumption. Note that the proposed ICAL scheme with a fully connected structure for a weighting coefficient, e.g.,  $\rho = 0.7$ , is capable of supporting both communications and localization, especially with higher transmit power. In particular, with 26 dBW transmit power, the proposed ICAL scheme with a fully connected structure can offer the sum SE of approximately 85 bps/Hz for all the UTs, and guarantee the localization precision  $< 5$  m for each UT, simultaneously. Besides, in the low region of the transmit power, the hybrid scheme with a partially connected structure for  $\rho = 0$  has better APEB performance than with a fully connected one for  $\rho = 0.7$ ,

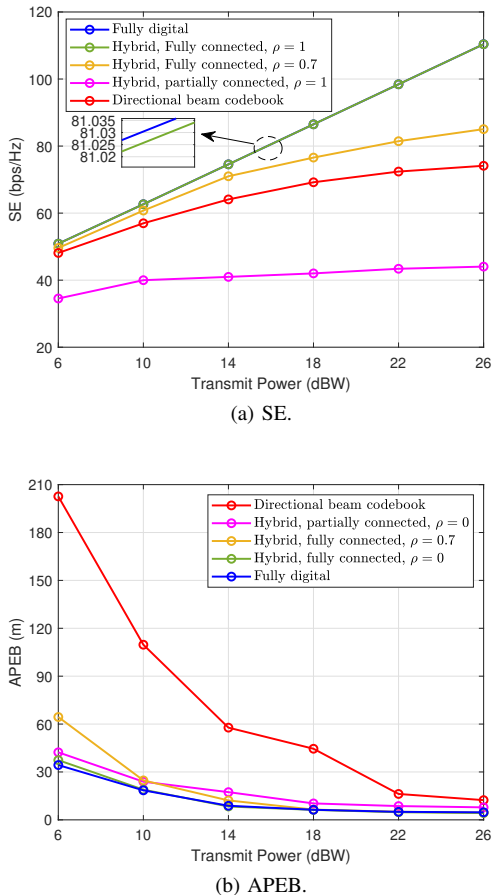


Fig. 7. SE and APEB performance versus transmit power  $P$  with  $N_t = 576$  antennas for different precoding design strategies.

at the cost of the SE performance. In general, the directional beam codebook-based precoder performs worst in the medium and high transmit power regions.

## VI. CONCLUSION

In this paper, we developed a system that is able to simultaneously perform communications and localization for massive MIMO LEO satellite ICAL systems, by exploiting sCSI. We derived the performance metrics SE and SPEB for communications and localization, respectively, based on which we formulated a multi-objective problem, to design the hybrid transmitter for the ICAL. Then, the SE and SPEB maximization problem was converted into the sum-MSE and Euclidean distance minimization one. We introduced a weighting coefficient to tradeoff between the performance of communications and localization, and formulated an algorithmic framework to handle the corresponding problem. Simulation results confirmed that the proposed scheme could simultaneously support the communications and localization operations. Moreover, in this paper, only a single LEO satellite was considered, and future works will focus on the cooperation of multiple satellites to further improve the communication capacity and localization accuracy.

## APPENDIX A

### EXPRESSION FOR THE MATRIX $\Xi_k$ IN (13)

We denote the rotated position vectors associated with the  $k$ th UT as  $\mathbf{p}_k^r \triangleq \mathbf{R}(\mathbf{o})^{-1}(\mathbf{p}_k - \mathbf{q}) \triangleq [p_k^{r,x}, p_k^{r,y}, p_k^{r,z}]^T$  [9], where  $\mathbf{R}(\mathbf{o})$  is the corresponding rotation matrix, given by [31], [71], [72]

$$\mathbf{R}(\mathbf{o}) \triangleq \begin{bmatrix} \cos \varphi_2 & -\sin \varphi_1 \sin \varphi_2 & \cos \varphi_1 \sin \varphi_2 \\ 0 & \cos \varphi_1 & \sin \varphi_1 \\ -\sin \varphi_2 & -\sin \varphi_1 \cos \varphi_2 & \cos \varphi_1 \cos \varphi_2 \end{bmatrix} \quad (39)$$

$$\triangleq [\mathbf{r}_1, \mathbf{r}_2, \mathbf{r}_3]. \quad (40)$$

Then, the relationship between the AoD pair and the position of the  $k$ th UT is given by [31], [71], [72]

$$\theta_k^x = \arctan\left(\frac{p_k^{r,z}}{p_k^{r,x}}\right), \quad \theta_k^y = \arccos\left(\frac{p_k^{r,y}}{\|\mathbf{p}_k^r\|_2}\right). \quad (41)$$

Besides, the propagation delay and Doppler shifts of LoS path correspond to the position and the velocity information of the  $k$ th UT as follows [73]

$$\tau_k = \frac{\|\mathbf{p}_k - \mathbf{q}\|_2}{c}, \quad (42)$$

$$\nu_k = -\frac{f_c \dot{\mathbf{p}}_k^T (\mathbf{p}_k - \mathbf{q})}{c \|\mathbf{p}_k - \mathbf{q}\|_2}. \quad (43)$$

Then, the component  $\Xi_k$  of the transformation matrix in (13) for the  $k$ th UT can be expressed as

$$\Xi_k = \begin{bmatrix} \frac{\partial \theta_k^x}{\partial \mathbf{p}_k} & \frac{\partial \theta_k^y}{\partial \mathbf{p}_k} & \frac{\partial \tau_k}{\partial \mathbf{p}_k} & \frac{\partial \nu_k}{\partial \mathbf{p}_k} \end{bmatrix} \in \mathbb{R}^{3 \times 4}, \quad (44)$$

where the elements are detailed as

$$\frac{\partial \theta_k^x}{\partial \mathbf{p}_k} = \frac{p_k^{r,x} \mathbf{r}_3 - p_k^{r,z} \mathbf{r}_1}{(p_k^{r,x})^2 + (p_k^{r,z})^2}, \quad (45a)$$

$$\frac{\partial \theta_k^y}{\partial \mathbf{p}_k} = \frac{p_k^{r,y} (\mathbf{p}_k - \mathbf{q}) - \mathbf{r}_2 \|\mathbf{p}_k^r\|_2^2}{\|\mathbf{p}_k^r\|_2^2 \sqrt{(p_k^{r,x})^2 + (p_k^{r,z})^2}}, \quad (45b)$$

$$\frac{\partial \tau_k}{\partial \mathbf{p}_k} = \frac{1}{c} \frac{\mathbf{p}_k - \mathbf{q}}{\|\mathbf{p}_k - \mathbf{q}\|_2}, \quad (45c)$$

$$\frac{\partial \nu_k}{\partial \mathbf{p}_k} = \frac{f_c (\dot{\mathbf{p}}_k^T (\mathbf{p}_k - \mathbf{q})) (\mathbf{p}_k - \mathbf{q}) - \|\mathbf{p}_k - \mathbf{q}\|_2^2 \dot{\mathbf{p}}_k}{c \|\mathbf{p}_k - \mathbf{q}\|_2^3}. \quad (45d)$$

## APPENDIX B

### PROOF FOR EQ. (22)

The precoder  $\mathbf{W}_n^{\text{loc}}$  can be decomposed as

$$\mathbf{W}_n^{\text{loc}} = \mathbf{\Pi}_{\mathbf{L}_n} \mathbf{W}_n^{\text{loc}} + \mathbf{\Pi}_{\mathbf{L}_n}^\perp \mathbf{W}_n^{\text{loc}}, \quad (46)$$

where  $\mathbf{\Pi}_{\mathbf{L}_n} \triangleq \mathbf{L}_n (\mathbf{L}_n^H \mathbf{L}_n)^{-1} \mathbf{L}_n^H$  denotes the subspace spanned by the columns of  $\mathbf{L}_n$  and  $\mathbf{\Pi}_{\mathbf{L}_n}^\perp \triangleq \mathbf{I}_{N_t} - \mathbf{\Pi}_{\mathbf{L}_n}$ . Following the equality that  $\mathbf{C}_n = \mathbf{W}_n^{\text{loc}} (\mathbf{W}_n^{\text{loc}})^H$ , we have

$$\mathbf{C}_n = \mathbf{W}_n^{\text{loc}} (\mathbf{W}_n^{\text{loc}})^H = \mathbf{\Pi}_{\mathbf{L}_n} \mathbf{W}_n^{\text{loc}} (\mathbf{W}_n^{\text{loc}})^H (\mathbf{\Pi}_{\mathbf{L}_n})^H + \tilde{\mathbf{C}}_n, \quad (47)$$

It is worth noting that since  $\mathbf{v}_{k,n}$ ,  $\mathbf{v}_{k,n,\theta_k^x}$  and  $\mathbf{v}_{k,n,\theta_k^y}$  belong to the subspace  $\mathbf{\Pi}_{\mathbf{L}_n}$ , it is not difficult to verify that the terms  $\mathbf{v}_{k,n}^H \tilde{\mathbf{C}}_n \mathbf{v}_{k,n}$ ,  $\mathbf{v}_{k,n}^H \tilde{\mathbf{C}}_n \mathbf{v}_{k,n,\theta_k^x}$ ,  $\mathbf{v}_{k,n}^H \tilde{\mathbf{C}}_n \mathbf{v}_{k,n,\theta_k^y}$ ,  $\mathbf{v}_{k,n,\theta_k^x}^H \tilde{\mathbf{C}}_n \mathbf{v}_{k,n,\theta_k^x}$ ,  $\mathbf{v}_{k,n,\theta_k^y}^H \tilde{\mathbf{C}}_n \mathbf{v}_{k,n,\theta_k^y}$  are all

equal to zeros. Thus, it can be concluded that the FIM does not depend on  $\tilde{\mathbf{C}}_n$ . In addition, we have

$$\begin{aligned} \text{Tr}(\tilde{\mathbf{C}}_n) &= \text{Tr} \left( \mathbf{\Pi}_{\mathbf{L}_n} \mathbf{W}_n^{\text{loc}} (\mathbf{W}_n^{\text{loc}})^H \mathbf{\Pi}_{\mathbf{L}_n}^\perp \right. \\ &\quad \left. + \mathbf{\Pi}_{\mathbf{L}_n}^\perp \mathbf{W}_n^{\text{loc}} (\mathbf{W}_n^{\text{loc}})^H \mathbf{\Pi}_{\mathbf{L}_n} \right. \\ &\quad \left. + \mathbf{\Pi}_{\mathbf{L}_n}^\perp \mathbf{W}_n^{\text{loc}} (\mathbf{W}_n^{\text{loc}})^H \mathbf{\Pi}_{\mathbf{L}_n}^\perp \right) \\ &= \left\| (\mathbf{W}_n^{\text{loc}})^H \mathbf{\Pi}_{\mathbf{L}_n}^\perp \right\|_F^2 \geq 0. \end{aligned} \quad (48)$$

Furthermore,  $\mathbf{C}_n$  is subject to the constraint in Eq. (21b), and thus, it can be concluded that  $\text{Tr}(\tilde{\mathbf{C}}_n) = 0$ , otherwise the constraint in Eq. (21b) is not satisfied. As observed from Eq. (48),  $\text{Tr}(\tilde{\mathbf{C}}_n) = 0$  is equivalent to  $(\mathbf{W}_n^{\text{loc}})^H \mathbf{\Pi}_{\mathbf{L}_n}^\perp = 0$ , i.e.,  $\tilde{\mathbf{C}}_n = 0$ . Therefore,

$$\mathbf{C}_n = \mathbf{\Pi}_{\mathbf{L}_n} \mathbf{W}_n^{\text{loc}} (\mathbf{W}_n^{\text{loc}})^H (\mathbf{\Pi}_{\mathbf{L}_n})^H \triangleq \mathbf{L}_n \mathbf{Z}_n \mathbf{L}_n^H, \quad (49)$$

where  $\mathbf{Z}_n = (\mathbf{L}_n^H \mathbf{L}_n)^{-1} \mathbf{L}_n^H \mathbf{W}_n^{\text{loc}} (\mathbf{W}_n^{\text{loc}})^H \mathbf{L}_n (\mathbf{L}_n^H \mathbf{L}_n)^{-1}$ .

#### APPENDIX C

##### STEPS FOR HANDLING EQS. (31) – (37)

The steps for handling Eqs. (31) – (37) are presented as follows:

1) *Update of  $\mathbf{G}_{k,n}$* : We formulate the optimization problem to update  $\mathbf{G}_{k,n}$  as

$$\mathcal{Q}_4 : \underset{\mathcal{G}}{\text{minimize}} \quad f(\mathcal{G}) \quad (50a)$$

$$\text{s.t.} \quad \sum_{k=1}^K \sum_{n=1}^{N_{\text{sc}}} \text{Tr} \{ \mathbf{G}_{k,n} \mathbf{G}_{k,n}^H \} \leq PK. \quad (50b)$$

To handle problem  $\mathcal{Q}_4$ , we introduce a Lagrange multiplier for constraint in (50b) and the corresponding Lagrange function for  $\mathcal{Q}_4$  is given by [54]

$$\begin{aligned} f(\mathcal{G}, \mu) &= \sum_{k=1}^K \sum_{n=1}^{N_{\text{sc}}} L(\mathbf{G}_{k,n}) \\ &\quad + \mu \left( \sum_{k=1}^K \sum_{n=1}^{N_{\text{sc}}} \text{Tr} \{ \mathbf{G}_{k,n} \mathbf{G}_{k,n}^H \} - PK \right). \end{aligned} \quad (51)$$

Subsequently, by utilizing the Karush-Kuhn-Tucker (KKT) conditions of  $\mathcal{Q}_4$ ,  $\mathbf{G}_{k,n}$  can be updated by  $\mathbf{G}_{k,n} = (\mathbf{A}_{k,n} + \mu \mathbf{I}_{N_t})^{-1} \mathbf{\Psi}_{k,n}$ , where  $\mathbf{A}_{k,n}$  is a Hermitian matrix which can be decomposed as  $\mathbf{A}_{k,n} = \mathbf{D}_{k,n} \mathbf{\Lambda}_{k,n} \mathbf{D}_{k,n}^H$  and the expression for  $\mathbf{A}_{k,n}$ ,  $\mathbf{\Psi}_{k,n}$  is given by

$$\mathbf{A}_{k,n} = \rho \omega_{k,n} |u_{k,n}|^2 \bar{\mathbf{h}}_{k,n}^* \bar{\mathbf{h}}_{k,n}^T + \left( \frac{1-\rho}{K} + \frac{\eta_{k,n}}{2} \right) \mathbf{I}_{N_t}, \quad (52)$$

$$\begin{aligned} \mathbf{\Psi}_{k,n} &= \frac{1-\rho}{K} \mathbf{W}_n^{\text{loc}} + \rho \omega_{k,n} u_{k,n}^* \bar{\mathbf{h}}_{k,n}^* \mathbf{e}_k^T \\ &\quad + \frac{\eta_{k,n}}{2} (\mathbf{W}_{\text{RF}} \mathbf{W}_{\text{BB},n} - \mathbf{Q}_{k,n}). \end{aligned} \quad (53)$$

Then, the left hand side of Eq. (50b) can be written as a function of  $\mu$ , which is given by

$$\delta(\mu) = \sum_{k=1}^K \sum_{n=1}^{N_{\text{sc}}} \text{Tr} \{ \mathbf{G}_{k,n}(\mu) \mathbf{G}_{k,n}^H(\mu) \}$$

$$= \sum_{k=1}^K \sum_{n=1}^{N_{\text{sc}}} \sum_{i=1}^{N_t} \frac{[\Phi_{k,n}]_{i,i}}{([\mathbf{A}_{k,n}]_{i,i} + \mu)^2}, \quad (54)$$

where  $\Phi_{k,n} = \mathbf{D}_{k,n}^H \mathbf{\Psi}_{k,n} \mathbf{\Psi}_{k,n}^H \mathbf{D}_{k,n}$ . The Lagrange multiplier  $\mu$  can be found to satisfy the complementarity slackness condition [54]. In particular, if  $\delta(0) \leq PK$ , then  $\mu = 0$ ; otherwise  $\mu$  is selected to satisfy  $\delta(\mu) = PK$  via the bisection search.

2) *Update of  $u_{k,n}$* : The update for  $u_{k,n}$  is  $u_{k,n} = \mathbf{e}_k^T \mathbf{G}_{k,n}^H \bar{\mathbf{h}}_{k,n}^* (\sum_{i=1}^K |\bar{\mathbf{h}}_{k,n}^T \mathbf{G}_{k,n} \mathbf{e}_i|^2 + N_0)^{-1}$ .

3) *Update of  $\omega_{k,n}$* : The update for  $\omega_{k,n}$  is given by  $\omega_{k,n} = (|u_{k,n}^* \bar{\mathbf{h}}_{k,n}^T \mathbf{G}_{k,n} \mathbf{e}_k - 1|^2 + \sum_{i \neq k} |u_{k,n}^* \bar{\mathbf{h}}_{k,n}^T \mathbf{G}_{k,n} \mathbf{e}_i|^2 + N_0 |u_{k,n}|^2)^{-1}$ ,  $\forall k, n$ .

4) *Update of  $\mathbf{W}_{\text{BB},n}$* : The optimization problem to update  $\mathbf{W}_{\text{BB},n}$  is formulated as

$$\begin{aligned} \mathcal{Q}_5 : \underset{\{\mathbf{W}_{\text{BB},n}\}_{n=1}^{N_{\text{sc}}}}{\text{maximize}} \quad & f(\bar{\mathbf{W}}_{\text{BB}}) = \sum_{k=1}^K \sum_{n=1}^{N_{\text{sc}}} \frac{\eta_{k,n}}{2} \|\mathbf{G}_{k,n} \\ & - \mathbf{W}_{\text{RF}} \mathbf{W}_{\text{BB},n} + \mathbf{Q}_{k,n}\|_F^2. \end{aligned} \quad (55)$$

For both fully and partially connected structures, we set the derivative of the objective function  $f(\bar{\mathbf{W}}_{\text{BB}})$  with respect to  $\mathbf{W}_{\text{BB},i}$  to be zero, and then, the expression to update  $\mathbf{W}_{\text{BB},i}$  is given by  $\mathbf{W}_{\text{BB},i} = \frac{1}{\sum_{k=1}^K \eta_{k,i}} (\mathbf{W}_{\text{RF}}^H \mathbf{W}_{\text{RF}})^{-1} \sum_{k=1}^K \eta_{k,i} \mathbf{W}_{\text{RF}}^H (\mathbf{G}_{k,i} + \mathbf{Q}_{k,i})$ . In particular, for partially connected structure, we have  $\mathbf{W}_{\text{RF}}^H \mathbf{W}_{\text{RF}} = N_g \mathbf{I}_{N_{\text{rf}}}$ .

5) *Update of  $\mathbf{W}_{\text{RF}}$* : The optimization problem to update  $\mathbf{W}_{\text{RF}}$  is formulated as

$$\begin{aligned} \mathcal{Q}_6 : \underset{\mathbf{W}_{\text{RF}}}{\text{maximize}} \quad & \sum_{k=1}^K \sum_{n=1}^{N_{\text{sc}}} \frac{\eta_{k,n}}{2} \|\mathbf{G}_{k,n} - \mathbf{W}_{\text{RF}} \mathbf{W}_{\text{BB},n} \\ & + \mathbf{Q}_{k,n}\|_F^2 \end{aligned} \quad (56a)$$

s.t.  $\mathbf{W}_{\text{RF}} \in \mathcal{S}$ . (56b)

For the fully connected structure,  $\mathbf{W}_{\text{RF}}$  can be updated as  $\mathbf{W}_{\text{RF}} = \exp\{-j\angle \mathbf{X}^T\}$  [74], where  $\mathbf{X} = \sum_{k=1}^K \sum_{n=1}^{N_{\text{sc}}} \frac{\eta_{k,n}}{2} \mathbf{W}_{\text{BB},n} (\mathbf{G}_{k,n} + \mathbf{Q}_{k,n})^H - (\mathbf{T} - \lambda_{\max}(\mathbf{T}) \mathbf{I}_{N_{\text{rf}}}) \mathbf{W}_{\text{RF}}^H$  and  $\lambda_{\max}(\mathbf{T})$  denotes the maximum eigenvalue of  $\mathbf{T} = \sum_{k=1}^K \sum_{n=1}^{N_{\text{sc}}} \frac{\eta_{k,n}}{2} \mathbf{W}_{\text{BB},n} \mathbf{W}_{\text{BB},n}^H$  [74]. For the partially connected structure, by expanding the objective in (56a) and utilizing the property that  $\mathbf{W}_{\text{RF}}^H \mathbf{W}_{\text{RF}} = N_g \mathbf{I}_{N_{\text{rf}}}$ , the problem can be rewritten as [75]

$$\begin{aligned} \mathcal{Q}_7 : \underset{[\mathbf{W}_{\text{RF}}]_{i,j}}{\text{maximize}} \quad & \Re \left\{ \text{Tr} \left\{ \mathbf{Y}_{i,j}^H [\mathbf{W}_{\text{RF}}]_{i,j}^* \right\} \right\} \end{aligned} \quad (57)$$

s.t.  $|\mathbf{W}_{\text{RF}}]_{i,j}| = 1, \forall i, \forall j = \lceil i/N_g \rceil$ , (58)

where  $\mathbf{Y}_{i,j} = \sum_{k=1}^K \sum_{n=1}^{N_{\text{sc}}} \frac{\eta_{k,n}}{2} [\mathbf{G}_{k,n} + \mathbf{Q}_{k,n}]_{i,:} [\mathbf{W}_{\text{BB},n}]_{j,:}^H$ . Then, the  $(i, j)$ th element of  $\mathbf{W}_{\text{RF}}$  can be updated by  $[\mathbf{W}_{\text{RF}}]_{i,j} = \exp\{\angle \mathbf{Y}_{i,j}\}$ ,  $\forall i, \forall j = \lceil i/N_g \rceil$ .

#### REFERENCES

- [1] X. Qiang, L. You, Y. Zhu, F. Jiang, C. G. Tsinos, W. Wang, H. Wymeersch, and X. Q. Gao, "Hybrid precoding for integrated communications and localization in massive MIMO LEO satellite systems," in *Proc. IEEE ICC*, Rome, Italy, 2023, pp. 1–6.

- [2] X. You, C.-X. Wang, J. Huang, X. Q. Gao, Z. Zhang, M. Wang, Y. Huang, C. Zhang, Y. Jiang, J. Wang, and Z. Min, "Towards 6G wireless communication networks: Vision, enabling technologies, and new paradigm shifts," *Sci. China Inf. Sci.*, vol. 64, no. 1, pp. 1–74, 2021.
- [3] C. De Lima, D. Belot, R. Berkvens, A. Bourdoux, D. Dardari, M. Guillaud, M. Isomursu, E.-S. Lohan, Y. Miao, A. N. Barreto, M. R. K. Aziz, J. Saloranta, T. Sanguanpuak, H. Srieddeen, G. Seco-Granados, J. Sutuala, T. Svensson, M. Valkama, B. Van Liempd, and H. Wymeersch, "Convergent communication, sensing and localization in 6G systems: An overview of technologies, opportunities and challenges," *IEEE Access*, vol. 9, pp. 26902–26925, Feb. 2021.
- [4] Z. Xiao and Y. Zeng, "An overview on integrated localization and communication towards 6G," *Sci. China Inf. Sci.*, vol. 65, no. 3, pp. 1–46, Mar. 2022.
- [5] A. Liu, Z. Huang, M. Li, Y. Wan, W. Li, T. X. Han, C. Liu, R. Du, D. K. P. Tan, J. Lu, Y. Shen, F. Colone, and K. Chetty, "A survey on fundamental limits of integrated sensing and communication," *IEEE Commun. Surveys Tuts.*, vol. 24, no. 2, pp. 994–1034, 2nd Quart. 2022.
- [6] Y. Ye, L. You, J. Wang, H. Xu, K.-K. Wong, and X. Q. Gao, "Fluid antenna-assisted MIMO transmission exploiting statistical CSI," *IEEE Commun. Lett.*, vol. 28, no. 1, pp. 223–227, Jan. 2024.
- [7] S. Jeong, O. Simeone, A. Haimovich, and J. Kang, "Beamforming design for joint localization and data transmission in distributed antenna system," *IEEE Trans. Veh. Technol.*, vol. 64, no. 1, pp. 62–76, Jan. 2014.
- [8] S. Jeong, O. Simeone, and J. Kang, "Optimization of massive full-dimensional MIMO for positioning and communication," *IEEE Trans. Wireless Commun.*, vol. 17, no. 9, pp. 6205–6217, Sep. 2018.
- [9] G. Kwon, A. Conti, H. Park, and M. Win, "Joint communication and localization in millimeter wave networks," *IEEE J. Sel. Topics Signal Process.*, vol. 15, no. 6, pp. 1439–1454, Nov. 2021.
- [10] W. Li, Y. Liu, X. Li, and Y. Shen, "Three-dimensional cooperative localization via space-air-ground integrated networks," *China Commun.*, vol. 19, no. 1, pp. 253–263, Jan. 2022.
- [11] W. Wang, T. Chen, R. Ding, G. Seco-Granados, L. You, and X. Q. Gao, "Location-based timing advance estimation for 5G integrated LEO satellite communications," *IEEE Trans. Veh. Technol.*, vol. 70, no. 6, pp. 6002–6017, May 2021.
- [12] L. You, X. Qiang, K.-X. Li, C. G. Tsinos, W. Wang, X. Q. Gao, and B. Ottersten, "Hybrid analog/digital precoding for downlink massive MIMO LEO satellite communications," *IEEE Trans. Wireless Commun.*, vol. 21, no. 8, pp. 5962–5976, Aug. 2022.
- [13] A. Guidotti, C. Amatetti, F. Arnal, B. Chamaillard, and A. Vanelli-Coralli, "Location-assisted precoding in 5G LEO systems: Architectures and performances," in *Proc. Joint EuCNC/6G Summit*, Grenoble, France, Jul. 2022, pp. 154–159.
- [14] H. Al-Hraishawi, S. Chatzinotas, and B. Ottersten, "Broadband non-stationary satellite communication systems: Research challenges and key opportunities," in *Proc. IEEE ICC Workshops*, Montreal, QC, Canada, Jul. 2021, pp. 1–6.
- [15] F. S. Prol, R. M. Ferre, Z. Saleem, P. Välisuo, C. Pinell, E. S. Lohan, M. Elsanhoury, M. Elmusrati, S. Islam, K. Çelikbilek, K. Selvan, J. Yliaho, K. Rutledge, A. Ojala, L. Ferranti, J. Praks, M. Z. H. Bhuiyan, S. Kaasalainen, and H. Kuusniemi, "Position, navigation, and timing (PNT) through low earth orbit (LEO) satellites: A survey on current status, challenges, and opportunities," *IEEE Access*, vol. 10, pp. 83971–84002, Jul. 2022.
- [16] W. Wang, Y. Tong, L. Li, A.-A. Lu, L. You, and X. Q. Gao, "Near optimal timing and frequency offset estimation for 5G integrated LEO satellite communication system," *IEEE Access*, vol. 7, pp. 113298–113310, Aug. 2019.
- [17] L. You, K.-X. Li, J. Wang, X. Q. Gao, X.-G. Xia, and B. Ottersten, "Massive MIMO transmission for LEO satellite communications," *IEEE J. Sel. Areas Commun.*, vol. 38, no. 8, pp. 1851–1865, Aug. 2020.
- [18] A. Shahmansoori, G. E. Garcia, G. Destino, G. Seco-Granados, and H. Wymeersch, "Position and orientation estimation through millimeter-wave MIMO in 5G systems," *IEEE Trans. Wireless Commun.*, vol. 17, no. 3, pp. 1822–1835, Mar. 2018.
- [19] R. Mendrzik, H. Wymeersch, G. Bauch, and Z. Abu-Shaban, "Harnessing NLOS components for position and orientation estimation in 5G millimeter wave MIMO," *IEEE Trans. Wireless Commun.*, vol. 18, no. 1, pp. 93–107, Jan. 2018.
- [20] Z. Xiao, Z. Han, A. Nallanathan, O. A. Dobre, B. Clerckx, J. Choi, C. He, and W. Tong, "Antenna array enabled space/air/ground communications and networking for 6G," *IEEE J. Sel. Areas Commun.*, vol. 40, no. 10, pp. 2773–2804, Oct. 2022.
- [21] O. El Ayach, S. Rajagopal, S. Abu-Surra, Z. Pi, and R. W. Heath, "Spatially sparse precoding in millimeter wave MIMO systems," *IEEE Trans. Wireless Commun.*, vol. 13, no. 3, pp. 1499–1513, Mar. 2014.
- [22] J. Rachel, "AST SpaceMobile deploys massive array ahead of Sat to cell tests," <https://www.satellitetoday.com/telecom/2022/11/14/ast-space-mobile-deploys-massive-array-ahead-of-sat-to-cell-tests/>, Nov. 2022.
- [23] Z. Xiao, J. Yang, T. Mao, C. Xu, R. Zhang, Z. Han, and X.-G. Xia, "LEO satellite access network (LEO-SAN) towards 6G: Challenges and approaches," *IEEE Wireless Commun.*, 2022.
- [24] K.-X. Li, L. You, J. Wang, X. Q. Gao, C. G. Tsinos, S. Chatzinotas, and B. Ottersten, "Downlink transmit design in massive MIMO LEO satellite communications," *IEEE Trans. Commun.*, vol. 70, no. 2, pp. 1014–1028, Feb. 2022.
- [25] L. You, X. Qiang, K.-X. Li, C. G. Tsinos, W. Wang, X. Gao, and B. Ottersten, "Massive MIMO hybrid precoding for LEO satellite communications with twin-resolution phase shifters and nonlinear power amplifiers," *IEEE Trans. Commun.*, vol. 70, no. 8, pp. 5543–5557, Aug. 2022.
- [26] D. G. Riviello, B. Ahmad, A. Guidotti, and A. Vanelli-Coralli, "Joint graph-based user scheduling and beamforming in LEO-MIMO satellite communication systems," in *Proc. IEEE ASMS/SPSC*, Graz, Austria, Oct. 2022, pp. 1–8.
- [27] M. R. Dakkak, D. G. Riviello, A. Guidotti, and A. Vanelli-Coralli, "Evaluation of multi-user multiple-input multiple-output digital beamforming algorithms in B5G/6G low Earth orbit satellite systems," *Int J. Satell. Commun. N.*, pp. 1–17, Aug. 2023.
- [28] K.-X. Li, J. Wang, X. Q. Gao, C. G. Tsinos, and B. Ottersten, "Uplink transmit design for massive MIMO LEO satellite communications," *arXiv:2201.12940*, 2022.
- [29] Y. Shen and M. Z. Win, "Fundamental limits of wideband localization – Part I: A general framework," *IEEE Trans. Inf. Theory*, vol. 56, no. 10, pp. 4956–4980, Oct. 2010.
- [30] Y. Shen, H. Wymeersch, and M. Z. Win, "Fundamental limits of wideband localization – Part II: Cooperative networks," *IEEE Trans. Inf. Theory*, vol. 56, no. 10, pp. 4981–5000, Oct. 2010.
- [31] Z. Abu-Shaban, X. Zhou, T. Abhayapala, G. Seco-Granados, and H. Wymeersch, "Error bounds for uplink and downlink 3D localization in 5G millimeter wave systems," *IEEE Trans. Wireless Commun.*, vol. 17, no. 8, pp. 4939–4954, Aug. 2018.
- [32] A. Guerra, F. Guidi, and D. Dardari, "Single-anchor localization and orientation performance limits using massive arrays: MIMO vs. beamforming," *IEEE Trans. Wireless Commun.*, vol. 17, no. 8, pp. 5241–5255, Aug. 2018.
- [33] A. Kakkavas, M. H. C. García, R. A. Stirling-Gallacher, and J. A. Nossek, "Performance limits of single-anchor millimeter-wave positioning," *IEEE Trans. Wireless Commun.*, vol. 18, no. 11, pp. 5196–5210, Nov. 2019.
- [34] G. Maral, M. Bousquet, and Z. Sun, *Satellite Communications Systems: Systems, Techniques and Technology*. Hoboken, NJ, USA: John Wiley & Sons, 2020.
- [35] N. Garcia, H. Wymeersch, and D. T. Slock, "Optimal precoders for tracking the AoD and AoA of a mmWave path," *IEEE Trans. Signal Process.*, vol. 66, no. 21, pp. 5718–5729, Nov. 2018.
- [36] L. You, X. Qiang, C. G. Tsinos, F. Liu, W. Wang, X. Gao, and B. Ottersten, "Beam squint-aware integrated sensing and communications for hybrid massive MIMO LEO satellite systems," *IEEE J. Sel. Areas Commun.*, vol. 40, no. 10, pp. 2994–3009, Oct. 2022.
- [37] T. Chen, W. Wang, R. Ding, G. Seco-Granados, L. You, and X. Gao, "Precoding design for joint synchronization and positioning in 5G integrated satellite communications," in *Proc IEEE GLOBECOM*, Madrid, Spain, Dec. 2021, pp. 01–06.
- [38] H. Yuan, N. Yang, K. Yang, C. Han, and J. An, "Hybrid beamforming for terahertz multi-carrier systems over frequency selective fading," *IEEE Trans. Commun.*, vol. 68, no. 10, Oct. 2020.
- [39] Y. Zhu, P.-Y. Kam, and Y. Xin, "On the mutual information distribution of MIMO Rician fading channels," *IEEE Trans. Commun.*, vol. 57, no. 5, pp. 1453–1462, May 2009.
- [40] A. Stamoulis, S. N. Diggavi, and N. Al-Dahir, "Intercarrier interference in MIMO OFDM," *IEEE Trans. Signal Process.*, vol. 50, no. 10, pp. 2451–2464, Oct. 2002.
- [41] A. Papathanassiou, A. K. Salkintzis, and P. T. Mathiopoulos, "A comparison study of the uplink performance of W-CDMA and OFDM for mobile multimedia communications via LEO satellites," *IEEE Pers. Commun.*, vol. 8, no. 3, pp. 35–43, Jun. 2001.

- [42] Y. Lin, S. Jin, M. Matthaiou, and X. You, "Tensor-based channel estimation for millimeter wave MIMO-OFDM with dual-wideband effects," *IEEE Trans. Commun.*, vol. 68, no. 7, pp. 4218–4232, Jul. 2020.
- [43] C. Sun, X. Q. Gao, S. Jin, M. Matthaiou, Z. Ding, and C. Xiao, "Beam division multiple access transmission for massive MIMO communications," *IEEE Trans. Commun.*, vol. 63, no. 6, pp. 2170–2184, Jun. 2015.
- [44] M. Matthaiou, Y. Kopsinis, D. I. Laurenson, and A. M. Sayeed, "Ergodic capacity upper bound for dual MIMO Ricean systems: Simplified derivation and asymptotic tightness," *IEEE Trans. Commun.*, vol. 57, no. 12, pp. 3589–3596, Dec. 2009.
- [45] S. M. Kay, *Fundamentals of Statistical Signal Processing: Detection Theory*. Englewood Cliffs, NJ, USA: Prentice Hall, 1993.
- [46] W. Zhang and W. P. Tay, "Using reconfigurable intelligent surfaces for UE positioning in mmWave MIMO systems," *arXiv:2112.00256*, 2021.
- [47] R. T. Marler and J. S. Arora, "Survey of multi-objective optimization methods for engineering," *Struct. Multidisciplinary Optim.*, vol. 26, no. 6, pp. 369–395, Mar. 2004.
- [48] E. Björnson, E. A. Jorswieck, M. Debbah, and B. Ottersten, "Multiobjective signal processing optimization: The way to balance conflicting metrics in 5G systems," *IEEE Signal Process. Mag.*, vol. 31, no. 6, pp. 14–23, Nov. 2014.
- [49] K. P. Yoon and C.-L. Hwang, *Multiple attribute decision making: an introduction*. London, UK: Sage publications, 1995.
- [50] T. Saaty, "A scaling method for priorities in hierarchies, multiple objectives and fuzzy sets," *J. Math. Psych.*, vol. 15, no. 3, pp. 234–281, 1977.
- [51] Q. Shi, M. Razaviyayn, Z.-Q. Luo, and C. He, "An iteratively weighted MMSE approach to distributed sum-utility maximization for a MIMO interfering broadcast channel," *IEEE Trans. Signal Process.*, vol. 59, no. 9, pp. 4331–4340, Sep. 2011.
- [52] W. W.-L. Li, Y. Shen, Y. J. Zhang, and M. Z. Win, "Robust power allocation for energy-efficient location-aware networks," *IEEE/ACM Trans. Netw.*, vol. 21, no. 6, pp. 1918–1930, Dec. 2013.
- [53] F. Keskin, F. Jiang, F. Munier, G. Seco-Granados, and H. Wymeersch, "Optimal spatial signal design for mmWave positioning under imperfect synchronization," *IEEE Trans. Veh. Technol.*, vol. 71, no. 5, pp. 5558–5563, May 2022.
- [54] S. Boyd and L. Vandenberghe, *Convex Optimization*. New York, NY, USA: Cambridge Univ. Press, 2004.
- [55] J. Li, L. Xu, P. Stoica, K. W. Forsythe, and D. W. Bliss, "Range compression and waveform optimization for MIMO radar: A Cramér-Rao bound based study," *IEEE Trans. Signal Process.*, vol. 56, no. 1, pp. 218–232, Jan. 2008.
- [56] Y. Sun, P. Babu, and D. P. Palomar, "Majorization-minimization algorithms in signal processing, communications, and machine learning," *IEEE Trans. Signal Process.*, vol. 65, no. 3, pp. 794–816, Feb. 2017.
- [57] L. Vandenberghe and S. Boyd, "Semidefinite programming," *SIAM Rev.*, vol. 38, no. 1, pp. 49–95, Mar. 1996.
- [58] A. Kakkavas, G. Seco-Granados, H. Wymeersch, M. H. C. Garcia, R. A. Stirling-Gallacher, and J. A. Nossek, "5G downlink multi-beam signal design for LOS positioning," in *Proc. IEEE GLOBECOM*, Waikoloa, HI, USA, Feb. 2019, pp. 1–6.
- [59] M. W. Jacobson and J. A. Fessler, "An expanded theoretical treatment of iteration-dependent majorize-minimize algorithms," *IEEE Trans. Image Process.*, vol. 16, no. 10, pp. 2411–2422, Oct. 2007.
- [60] G. H. Golub and C. F. Van Loan, *Matrix Computations*. Baltimore, MD, USA: The Johns Hopkins Univ. Press, 2013.
- [61] Z.-Q. Luo, W.-K. Ma, A. M.-C. So, Y. Ye, and S. Zhang, "Semidefinite relaxation of quadratic optimization problems," *IEEE Signal Process. Mag.*, vol. 27, no. 3, pp. 20–34, May 2010.
- [62] N. Kishore Kumar and J. Schneider, "Literature survey on low rank approximation of matrices," *Linear and Multilinear Algebra*, vol. 65, no. 11, pp. 2212–2244, 2017.
- [63] Q. Wan, J. Fang, Z. Chen, and H. Li, "Hybrid precoding and combining for millimeter wave/sub-THz MIMO-OFDM systems with beam squint effects," *IEEE Trans. Veh. Technol.*, vol. 70, no. 8, pp. 8314–8319, Aug. 2021.
- [64] Z. Cheng, Z. He, and B. Liao, "Hybrid beamforming design for OFDM dual-function radar-communication system," *IEEE J. Sel. Topics Signal Process.*, vol. 15, no. 6, pp. 1455–1467, Oct. 2021.
- [65] S. Boyd, N. Parikh, E. Chu, B. Peleato, and J. Eckstein, "Distributed optimization and statistical learning via the alternating direction method of multipliers," *Found. Trends Mach. Learn.*, vol. 3, no. 1, pp. 1–122, Jul. 2011.
- [66] D. P. Bertsekas, *Nonlinear Programming*. Belmont, MA, USA: Athena Scientific, 1999.
- [67] M. Hong, Z.-Q. Luo, and M. Razaviyayn, "Convergence analysis of alternating direction method of multipliers for a family of nonconvex problems," *SIAM J. Optim.*, vol. 26, no. 1, pp. 337–364, 2016.
- [68] 3GPP TR 38.821 V16.1.0, "3rd Generation Partnership Project; Technical Specification Group Radio Access Network; Solutions for NR to support non-terrestrial networks (NTN) (Release 16)," Tech. Rep., May 2021.
- [69] 3GPP TR 38.211 V16.8.0, "3rd Generation Partnership Project; Technical Specification Group Radio Access Network; NR; Physical channels and modulation (Release 16)," Tech. Rep., Dec. 2021.
- [70] E. Lutz, M. Werner, and A. Jahn, *Satellite Systems for Personal and Broadband Communications*. Berlin, Germany: Springer Science & Business Media, 2012.
- [71] J. Vince, *Rotation Transforms for Computer Graphics*. London, U.K.: Springer Science & Business Media, 2011.
- [72] H. Chen, H. Sarrideen, T. Ballal, H. Wymeersch, M.-S. Alouini, and T. Y. Al-Naffouri, "A tutorial on terahertz-band localization for 6G communication systems," *IEEE Commun. Surveys Tuts.*, vol. 24, no. 3, pp. 1780–1815, 3rd Quart. 2022.
- [73] Z. Abu-Shaban, G. Seco-Granados, C. R. Benson, and H. Wymeersch, "Performance analysis for autonomous vehicle 5G-assisted positioning in GNSS-challenged environments," in *Proc. IEEE/ION PLANS*, Hilton Portland Downtown, Portland, Oregon, Apr. 2020, pp. 996–1003.
- [74] A. Arora, C. G. Tsinos, B. S. M. R. Rao, S. Chatzinotas, and B. Ottersten, "Hybrid transceivers design for large-scale antenna arrays using majorization-minimization algorithms," *IEEE Trans. Signal Process.*, vol. 68, pp. 701–714, Dec. 2019.
- [75] X. Yu, J.-C. Shen, J. Zhang, and K. B. Letaief, "Alternating minimization algorithms for hybrid precoding in millimeter wave MIMO systems," *IEEE J. Sel. Topics Signal Process.*, vol. 10, no. 3, pp. 485–500, Apr. 2016.